



Systems metabolic engineering of *Corynebacterium glutamicum* eliminates all by-products for selective and high-yield production of the platform chemical 5-aminovalerate

Christina Rohles¹, Sarah Pauli¹, Gideon Gießelmann, Michael Kohlstedt, Judith Becker, Christoph Wittmann*

Institute of Systems Biotechnology, Saarland University, Germany

ARTICLE INFO

Keywords:

Bioeconomy
Lysine
Glutarate
Arginine
GABA permease
Import
Export
Fed-batch
Corynebacterium glutamicum
Systems metabolic engineering
Pseudomonas putida KT2440

ABSTRACT

5-aminovalerate (AVA) is a platform chemical of substantial commercial value to derive nylon-5 and five-carbon derivatives like δ -valerolactam, 1,5-pentanediol, glutarate, and 5-hydroxyvalerate. *De novo* bio-production synthesis of AVA using metabolically engineered cell factories is regarded as exemplary route to provide this chemical in a sustainable way. So far, this route is limited by low titers, rates and yields and suffers from high levels of by-products. To overcome these limitations, we developed a novel family of AVA producing *C. glutamicum* cell factories. Stepwise optimization included (i) improved AVA biosynthesis by expression balancing of the heterologous *davBA* genes from *P. putida*, (ii) reduced formation of the by-product glutarate by disruption of the catabolic γ -aminobutyrate pathway (iii), increased AVA export, and (iv) reduced AVA re-import via native and heterologous transporters to account for the accumulation of intracellular AVA up to 300 mM. Strain *C. glutamicum* AVA-5A, obtained after several optimization rounds, produced 48.3 g L⁻¹ AVA in a fed-batch process and achieved a high yield of 0.21 g g⁻¹. Surprisingly in later stages, the mutant suddenly accumulated glutarate to an extent equivalent to 30% of the amount of AVA formed, tenfold more than in the early process, displaying a severe drawback toward industrial production. Further exploration led to the discovery that ArgD, naturally aminating N-acetyl-L-ornithine during L-arginine biosynthesis, exhibits deaminating side activity on AVA towards glutarate formation. This promiscuity became relevant because of the high intracellular AVA level and the fact that ArgD became unoccupied with the gradually stronger switch-off of anabolism during production. Glutarate formation was favorably abolished in the advanced strains AVA-6A, AVA-6B, and AVA-7, all lacking *argD*. In a fed-batch process, *C. glutamicum* AVA-7 produced 46.5 g L⁻¹ AVA at a yield of 0.34 g g⁻¹ and a maximum productivity of 1.52 g L⁻¹ h⁻¹, outperforming all previously reported efforts and setting a milestone toward industrial manufacturing of AVA. Notably, the novel cell factories are fully genome-based, offering high genetic stability and requiring no selection markers

1. Introduction

Growing concerns about global warming, pollution, public health as well as rising prices and scarcity of fossil resources are major drivers towards a green and circular bio-industry (Kohlstedt et al., 2022). To obtain our everyday chemicals in a more sustainable way, great efforts are being made to replace traditional petroleum-based production with processes from renewable raw materials (Becker et al., 2013a). Meanwhile, bio-based production of dicarboxylic acids such as succinate

(Lange et al., 2017), glutarate (Rohles et al., 2018), *cis,cis*-muconate (Barton et al., 2018), and adipate (Vardon et al., 2015), as well as diamines like 1,3-diaminopropane (Chae et al., 2015) and 1,5-diaminopentane (Kind et al., 2010) successfully rivals petrochemical routes.

A chemical of great importance is 5-aminovalerate (AVA). The five-carbon non-proteinogenic amino acid is a building block for nylon-5, a tough fiber similar to nylon-6,6, but with lower crystallinity (Adkins et al., 2013). Moreover, nylon-5, as odd nylon, is a desirable ferroelectric material for sensors and dielectric energy storage media and, given these

* Corresponding author. Campus A1 5, 66123, Saarbrücken, Germany.

E-mail address: christoph.wittmann@uni-saarland.de (C. Wittmann).

¹ These authors contributed equally.

<https://doi.org/10.1016/j.ymben.2022.07.005>

Received 30 March 2022; Received in revised form 1 July 2022; Accepted 13 July 2022

Available online 30 July 2022

1096-7176/© 2022 The Author(s). Published by Elsevier Inc. on behalf of International Metabolic Engineering Society. This is an open access article under the CC BY-NC-ND license (<http://creativecommons.org/licenses/by-nc-nd/4.0/>).

remarkable properties, is currently experiencing a renaissance (von Tiedemann et al., 2020). The ability to convert AVA into five-carbon derivatives such as δ -valerolactam (Xu et al., 2020), 1,5-pentanediol (Cen et al., 2021), glutarate (Rohles et al., 2016), and 5-hydroxyvalerate (Sohn et al., 2021) makes this substance a platform chemical with substantial commercial value.

AVA is accessible through chemical synthesis from piperidine at attractive yield (Dairo et al., 2016). However, this process requires expensive catalysts and solvents, long reaction times and high temperatures, suffers from the lack of sustainability of the petrochemical feedstock, and is still at the feasibility stage. To this end, microbial production of AVA is regarded the most promising route to be established at industrial scale. Naturally, AVA occurs as an intermediate during degradation of L-lysine (Müller and Rodwell, 1971) (Fig. 1). In *Pseudomonas putida*, L-lysine is first decarboxylated into 5-aminovaleramide by L-lysine 2-monooxygenase (DavB). Subsequent deamination into AVA is catalyzed by 5-aminopentanamidase (DavA).

A number of studies have attempted to obtain AVA by biotransformation from L-lysine using heterologous expression of the genes *davBA* in *E. coli* (Li et al., 2016; Park et al., 2013, 2014; Wang et al., 2016). More recently, the 2-keto-6-aminocaproate pathway was established as another alternative route for fed-batch biotransformation from L-lysine (Cheng et al., 2021). All biotransformation processes require L-lysine as raw material, a global feed amino acid produced by fermentation in the volume of 5 million tons per year (Becker et al., 2018b). In a first phase, they are promising to build up the AVA market. However long-term, direct *de novo* synthesis of AVA from renewables appears much more attractive due to the simpler set-up and lower production costs, as compared to two stages of fermentation (Adkins et al., 2013). Notably, *C. glutamicum* efficiently synthesizes L-lysine from sugar, offering an attractive *de novo* access (Wittmann and Heinze, 2001). Towards *de novo* AVA synthesis, we previously upgraded the genome-based L-lysine hyperproducer *C. glutamicum* LYS-12 (Becker et al., 2011). Several rounds of optimization resulted in the genome-based cell factory *C. glutamicum* AVA-3 that expressed *davBA* in the genomic *bioD* locus and, after deletion, no longer expressed the genes *lysE* and *gabT* to reduce secretion of the undesired by-products L-lysine and glutarate (Rohles et al., 2016). In a molasses-based fed-batch, AVA-3 accumulated 28 g L⁻¹ AVA within 50 h, together with 7 g L⁻¹ glutarate. In another study, AVA production in an industrial L-lysine producing *C. glutamicum* strain (expressing *davBA* under a synthetic promoter and lacking *gabT*) yielded 33 g L⁻¹ AVA in 150 h, whereby glutarate and L-lysine were formed as by-products (Shin et al., 2016). Strain *C. glutamicum* KCTC 1857 produced 39.9 g L⁻¹ AVA in a fed-batch process over 74 h, along with 46 g L⁻¹ L-lysine (even more than the desired product) and lower amounts of glutarate (Shin et al., 2014). Up to now, the massive quantities of by-products have remained a challenge in *de novo* AVA production, greatly limiting AVA yields, titers, and selectivity.

Here, we created a family of superior *C. glutamicum* production strains for high-yield and high-level AVA production. The new strain design allowed AVA to be produced without by-products for the first time. *C. glutamicum* AVA-6B and AVA-7, obtained through iterative cycles of systems metabolic engineering, accumulated up to 48.3 g L⁻¹ AVA and achieved a high AVA yield of 0.56 mol mol⁻¹. In this regard, our development sets a new benchmark towards industrial AVA production.

2. Materials and methods

2.1. Strains and plasmids

C. glutamicum ATCC 13032 was obtained from the German Collection of Microorganisms and Cell Cultures (DSMZ, Braunschweig, Germany). The basic AVA producers *C. glutamicum* AVA-1, AVA-2, and AVA-3 were obtained from previous work (Rohles et al., 2016). *E. coli* DH5 α (Invitrogen, Karlsruhe, Germany) and *E. coli* NM522 (Stratagene,

Amsterdam, The Netherlands) were used for plasmid amplification and methylation, respectively. The integrative vector pClik int *sacB* was used for genomic modification of *C. glutamicum* (Buschke et al., 2011). The plasmid pTC was co-expressed in *E. coli* NM522 to methylate plasmid DNA (Kind et al., 2010). Strains were maintained as cryo stocks at -80 °C. Table 1 lists all strains and plasmids of this work, including newly derived derivatives.

2.2. Recombinant DNA work

For molecular design, Clone Manager Professional 9 (Sci-Ed Software, Denver, USA) was used. Genetic constructs for genomic integration of the *tuf* promoter from *C. glutamicum*, upstream of a selected target gene, comprised (i) 500 bp-sized flanking regions as homologous recombination sites and (ii) a 200 bp sized DNA fragment of the promoter of the structural *tuf* gene (NCgl0480) (Becker et al., 2005). Genetic constructs for genome-based expression of a newly introduced target sequence comprised (i) 500 bp-sized flanking regions as homologous recombination sites for the integration locus, (ii) a 200 bp sized DNA fragment of the promoter of the structural *tuf* gene, plus (iii) the gene(s) of interest. Genes within monocistronic modules were separated by a 20-bp sized ribosomal binding site as intergenic region (Rohles et al., 2016). Genetic constructs for genomic deletion of a target sequence comprised (i) 500 bp-sized flanking regions as homologous recombination sites upstream and downstream of the sequence to be deleted. In addition to the native *davBA* operon from *P. putida*, a codon-optimized version was created. For codon optimization, rare codons were replaced by more frequent ones, as done before (Kind et al., 2010). The relative adaptiveness of heterologous gene sequences to the codon usage of *C. glutamicum* was estimated using the Graphical Codon Usage Analyzer (Fuhrmann et al., 2004). Amplification and assembly of DNA fragments, amplification, purification, and transformation of plasmid vectors into *E. coli* and *C. glutamicum* strains, genomic recombination and strain validation were performed as described previously (Becker et al., 2013b; Giesselmann et al., 2019; Hoffmann et al., 2021). Details on the used protocols are provided in the primers, used for genetic engineering, are listed in the supplement (Table S1).

2.3. Growth medium

Pre-cultures of *C. glutamicum* were grown on BHI medium (37 g L⁻¹ BHI, Becton Dickinson). For BHI plate cultures, 20 g L⁻¹ agar was added (Difco Laboratories). The minimal medium, used for *C. glutamicum* pre-cultures and main cultures, contained 200 mM potassium phosphate (pH 7.8), 10 g of glucose, 15 g of (NH₄)₂SO₄, 1 g of NaCl, 200 mg of MgSO₄·7H₂O, 55 mg of CaCl₂, 30 mg of 3,4-dihydroxybenzoic acid, 20 mg of FeSO₄, 2 mg of FeCl₃·6H₂O, 2 mg of MnSO₄·H₂O, 0.5 mg of ZnSO₄·7H₂O, 0.2 mg of CuCl₂·2H₂O, 0.2 mg of Na₂B₄O₇·10H₂O, 0.1 mg of (NH₄)₆Mo₇O₂₄·4H₂O, 1 mg of thiamine-HCl, 1 mg of calcium pantothenate, and 0.5 mg of biotin per liter (Rohles et al., 2018). For tolerance testing, AVA was added up to a level of 200 g L⁻¹ from a pre-sterilized stock. To grow L-arginine-auxotrophic strains, yeast extract (Difco yeast extract, 1.5 g L⁻¹, Becton Dickinson), casamino acids (Bacto casamino acids, 2 g L⁻¹, Becton Dickinson), or L-arginine (200 mg L⁻¹), respectively, were added from pre-sterilized stocks.

2.4. Batch cultivation in shake flasks

A single colony, pre-incubated on BHI agar for 48 h at 30 °C, was used to inoculate a first pre-culture in BHI medium. After 15 h of incubation, cells were harvested (6000×g, 5 min, 20 °C), washed twice with minimal medium, inoculated into a second pre-culture in minimal medium, and grown overnight. Then, cells were harvested, washed as described above, and used to inoculate the main cultures. Cultivations were carried out on an orbital shaker (30 °C, 230 rpm, 50 mm shaking diameter, Multitron, Infors AG, Bottmingen, Switzerland) using baffled

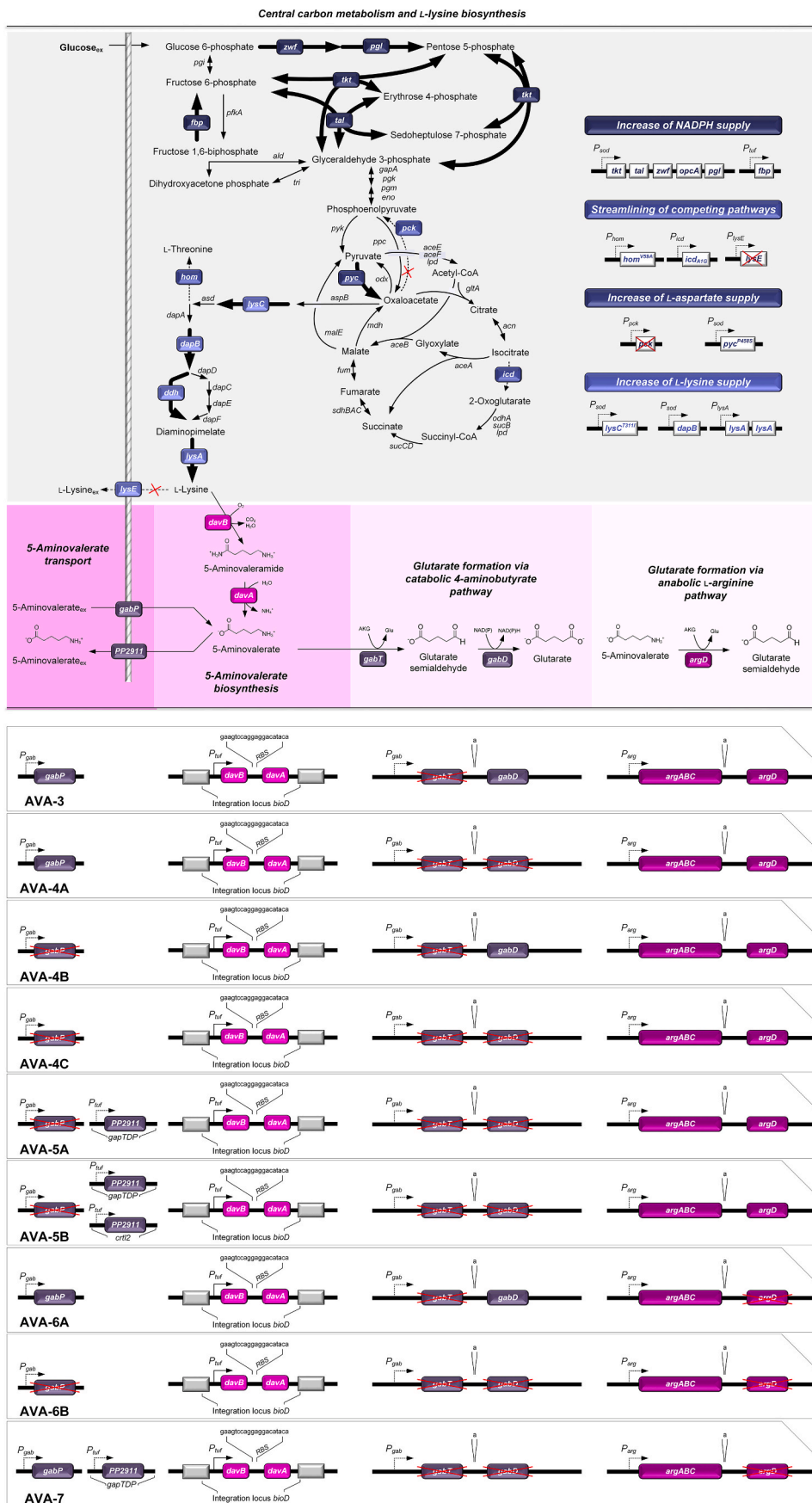


Fig. 1. Metabolic pathway design for the production of 5-aminovalerate (AVA) in *Corynebacterium glutamicum*. The overview illustrates the genomic layout of the AVA strain family, created in this work. For each AVA producer, we show the genetic changes in core carbon metabolism, L-lysine synthesis and secretion, AVA synthesis, AVA import and export, AVA withdrawal into glutarate via the catabolic *gap* pathway, and AVA withdrawal into glutarate via the anabolic L-arginine pathway. All modifications were implemented into the genome. The genes *davBA* from *P. putida* KT2440, encoding L-lysine monooxygenase (DavB) and 5-aminovaleramidase (DavA), were used to establish the biosynthetic AVA module. The two genes were integrated as a mono-cistronic operon under control of the constitutive *tuf*-promotor into the *bioD* locus of the L-lysine hyper-producer *C. glutamicum* LYS-12 (Rohles et al., 2016). The expression of *davBA* was further refactored by codon-optimization and the construction of a bicistronic operon (Table 2). Import and export of AVA were tackled by the elimination of the importer *gapP* and heterologous expression of GABA III permease from *P. putida* KT2440 in the *gabTDP* locus. Different combinations of the targets were evaluated. Other tested native AVA exporters, not shown here, are given in Table 1 and described in the text. The elimination of AVA withdrawal via the catabolic GABA pathway was approached by partial and complete deletion of the *gabTDP* operon. Different variants of the modules were tested for optimization. The elimination of AVA withdrawal via the anabolic L-arginine pathway was tackled by deleting *argD*. LYS-12 had been derived from the wild type before by the implementation of twelve genomic modifications before (Becker et al., 2011): overexpression of the *tkt* operon (P_{sod} *tkt*), overexpression of fructose 1,6-bisphosphatase (P_{inf} *fbp*), modification and amplification of pyruvate carboxylase (P_{sod} *pycA^{P458S}*), deletion of phosphoenolpyruvate carboxykinase (Δ *pck*), attenuation of isocitrate dehydrogenase (*icd^{att}*), modification and amplification of aspartokinase (P_{sod} *lysC^{T311H}*), attenuation of homoserine dehydrogenase (*hom^{V59A}*), amplification of 4-hydroxy-tetrahydrodipicolinate reductase (P_{sod} *dapB*), duplication of meso-diaminopimelate dehydrogenase (2x *ddh*), and duplication of meso-diaminopimelate decarboxylase (2x *lysA*).

Table 1
Strains and plasmids used in this study.

Strain	Description	Reference
<i>E. coli</i>		
DH5 α	<i>supE44</i> , Δ <i>lacU169</i> (ϕ 80 <i>lacZ</i> Δ M15), <i>hsdR17</i> (<i>rk-mk+</i>), <i>recA1</i> , <i>endA1</i> , <i>thi1</i> , <i>gyrA</i> , <i>relA</i>	Invitrogen
NM522	<i>F</i> <i>proA+</i> <i>B+</i> , <i>lacIq</i> , Δ (<i>lacZ</i>)M15/ Δ (<i>lac-proAB</i>), <i>glnV</i> , <i>thi-1</i> Δ (<i>hsdS-mcrB</i>)5	Stratagene
<i>C. glutamicum</i>		
ATCC 13032	Wild type (DSM 20300)	DSMZ
AVA-1	<i>C. glutamicum</i> LYS-12 with genomic expression of the native <i>P. putida</i> genes <i>davBA</i> under control of <i>P_{nif}</i>	Rohles et al. (2016)
AVA-2	AVA-1 Δ <i>lysE</i>	Rohles et al. (2016)
AVA-3	AVA-1 Δ <i>lysE</i> Δ <i>gabT</i>	Rohles et al. (2016)
AVA-1 <i>P_{nif}</i> <i>davBA</i> ^{opt}	LYS-12 with genomic expression of the monocistronic module <i>P_{nif}</i> <i>davBA</i> using codon-optimized <i>P. putida</i> genes	This work
AVA-1 <i>P_{nif}</i> <i>davB</i> <i>P_{nif}</i> <i>davA</i>	LYS-12 with genomic expression of the bicistronic module <i>P_{nif}</i> <i>davB</i> <i>P_{nif}</i> <i>davA</i> using the native <i>P. putida</i> genes	This work
AVA-2 Δ <i>aroP</i>	AVA-2 with genomic deletion of the amino acid permease NCgl1062 (<i>aroP</i>)	This work
AVA-2 Δ <i>pheP</i>	AVA-2 with genomic deletion of the amino acid permease NCgl1108 (<i>pheP</i>)	This work
AVA-2 Δ NCgl0453	AVA-2 with genomic deletion of the 4-aminobutyrate related permease NCgl0453	This work
AVA-2 Δ NCgl2936	AVA-2 with genomic deletion of the ABC transporter permease NCgl2936	This work
AVA-4A	AVA-3 with genomic deletion of glutarate semialdehyde dehydrogenase (<i>gabD</i>)	This work
AVA-4B	AVA-3 with genomic deletion of γ -aminobutyrate permease (<i>gabP</i>)	This work
AVA-4C	AVA-2 with genomic deletion of the catabolic γ -aminobutyrate operon (<i>gabTDP</i>)	This work
AVA-5A	AVA-4C with genomic expression of GABA III permease (PP2911) from <i>P. putida</i> KT2440 under control of <i>P_{nif}</i>	This work
AVA-5B	AVA-5A with genomic expression of a second copy of GABA III permease (PP2911) from <i>P. putida</i> KT2440 under control of <i>P_{nif}</i>	This work
AVA-6A	AVA-3 with genomic deletion of N-acetylornithine transaminase (<i>argD</i>)	This work
AVA-6B	AVA-4C with genomic deletion of <i>argD</i>	This work
AVA-7	AVA-6B with genomic expression of GABA III permease (PP2911) from <i>P. putida</i> KT2440 under control of <i>P_{nif}</i>	This work
AVA-8	AVA-7 with with genomic expression of a second copy of GABA III permease (PP2911) from <i>P. putida</i> KT2440 under control of <i>P_{nif}</i>	This work
Plasmids		
pTC15AcgIM	Co-expression of DNA methyltransferase in <i>E. coli</i> during cloning, ORI for <i>E. coli</i> , <i>tet^R</i>	Becker et al. (2011)
pClik 5a MCS	Episomal vector for expression in <i>C. glutamicum</i> , ORI for <i>E. coli</i> and <i>C. glutamicum</i> , MCS, <i>kan^R</i>	Becker et al. (2011)
pClik int <i>sacB</i>	Integrative vector for genomic modification of <i>C. glutamicum</i> , ORI for <i>E. coli</i> , MCS, <i>kan^R</i> , <i>sacB</i>	Becker et al. (2011)
pClik int <i>sacB</i> <i>P_{nif}</i> <i>davBA</i> ^{opt}	Genomic expression of <i>P_{nif}</i> <i>davBA</i> ^{opt} in the <i>bioD</i> locus	This work
pClik int <i>sacB</i> <i>P_{nif}</i> <i>davB</i> <i>P_{nif}</i> <i>davA</i>	Genomic expression of <i>P_{nif}</i> <i>davB</i> <i>P_{nif}</i> <i>davA</i> in the <i>bioD</i> locus	This work
pClik int <i>sacB</i> <i>P_{nif}</i> <i>davB</i> <i>P_{sod}</i> <i>davA</i>	Genomic expression of <i>P_{nif}</i> <i>davB</i> <i>P_{sod}</i> <i>davA</i> in the <i>bioD</i> locus	This work
pClik int <i>sacB</i> Δ <i>gabD</i>	Genomic deletion of <i>gabD</i>	This work
pClik int <i>sacB</i> Δ <i>gabP</i>	Genomic deletion of <i>gabP</i>	This work
	Genomic deletion of <i>gabTDP</i>	This work

Table 1 (continued)

Strain	Description	Reference
pClik int <i>sacB</i> Δ <i>gabTDP</i>		
pClik int <i>sacB</i> Δ NCgl0453	Genomic deletion of NCgl0453	This work
pClik int <i>sacB</i> Δ NCgl1062	Genomic deletion of NCgl1062	This work
pClik int <i>sacB</i> Δ NCgl1108	Genomic deletion of NCgl1108	This work
pClik int <i>sacB</i> Δ NCgl2355	Genomic deletion of NCgl2355	This work
pClik int <i>sacB</i> Δ <i>argD</i>	Genomic deletion of <i>argD</i>	This work
pClik int <i>sacB</i> <i>P_{nif}</i> <i>PP2911</i> (<i>gapTDP</i>)	Genomic replacement of <i>gabTDP</i> by <i>P_{nif}</i> <i>PP2911</i>	This work
pClik int <i>sacB</i> <i>P_{nif}</i> <i>PP2911</i> (<i>ctrl2</i>)	Genomic expression of <i>P_{nif}</i> <i>PP2911</i> in the <i>ctrl2</i> locus	This work

shake flasks that were filled with 10% of the total volume with medium. The experiments were conducted in triplicate.

2.5. Screening of strain robustness and nutrient demand in microbioreactors

Tolerance and medium testing was conducted in 48-well flower plates (MTP-48-B, m2p-labs, Baesweiler, Germany) using a high-throughput microbioreactor with on-line sensing of growth (1300 rpm, 30 °C, 85% humidity BioLector 1, Beckman Coulter) as described previously (Becker et al., 2018a). The inoculum was prepared in two steps as shown above. Each well was filled with 1 mL minimal medium. In selected cases, the medium was supplemented with glutarate, AVA, L-arginine, yeast extract, and/or casamino acids as described below. Experiments were conducted in triplicate.

2.6. Fed-batch production of AVA

C. glutamicum was benchmarked for its performance to produce AVA using 1 L lab-scale bioreactors (DASGIP Eppendorf, Jülich, Germany). The process was started with 300 mL glucose-based batch medium that contained 80 g of glucose, 25 g of (NH₄)₂SO₄, 15 g of yeast extract (Difco, Becton and Dickinson), 2 g of citrate, 1.25 g of KH₂PO₄, 1.25 g of Na₂HPO₄, 1.25 g of MgSO₄·7 H₂O, 165 mg of CaSO₄·2 H₂O, 70 mg of FeSO₄·7 H₂O, 30 mg of ZnSO₄·7 H₂O, 9 mg of MnSO₄·H₂O, 650 μ g of CoSO₄·5 H₂O, 600 μ g of CoSO₄·7 H₂O, 480 μ g of NiSO₄·6 H₂O, 400 μ g of boric acid, 85 μ g of Na₂MoO₄·2 H₂O, 30 mg of calcium pantothenate, 9 mg of nicotine amide, 7.5 mg of thiamine-HCl, 3 mg of biotin, and 1 mL of antifoam 204 (Sigma-Aldrich, Steinheim, Germany) per liter. The batch medium was additionally supplemented with 500 mg L⁻¹ L-arginine to ensure initial growth of L-arginine-auxotrophic strains. The inoculum was prepared by growing the selected strains on complex medium (37 g L⁻¹ of BHI, 10 g L⁻¹ yeast extract, and 20 g L⁻¹ glucose) on an orbital shaker as described above. After 24 h incubation, cells were harvested (6000 \times g, 5 min, 20 °C), resuspended in 10 mL batch medium, and added to the process. During the process, temperature (30 \pm 0.1 °C) and pH value (7.0 \pm 0.1, 25% NH₄OH) were automatically controlled by the inbuilt process software (DASware Control v. 5.6, DASGIP Eppendorf). The level of dissolved oxygen (DO) was monitored using an electrode (Hamilton) and kept above 30% saturation by automatic adjustment of stirrer speed (up to 1500 rpm) and aeration rate (up to 1 VVM). Strain AVA-5C revealed foam formation in later process stages which complicated the analysis of the optical density. To overcome this analytical problem, the aeration rate was halved to 0.5 VVM. For maintain sufficient aeration, the oxygen content in the inlet gas was doubled by mixing of air with pure oxygen. A feed phase was started, when the initially added glucose was depleted. The feed solution contained increased levels of glucose (600 g L⁻¹), (NH₄)₂SO₄ (200 g L⁻¹), and yeast extract (15 g L⁻¹), plus urea (14 g L⁻¹) as additional nitrogen

source. The concentration of the other components was the same as in the batch medium (see above). Feed pulses were automatically added, once the DO level increased above 45%. This procedure maintained the glucose level above 10 g L^{-1} . The fed-batch processes were conducted in duplicate.

2.7. Quantification of cells, substrates, and products

Cell concentration was measured photometrically at 660 nm (OD_{660}). Cell dry mass (CDM) was determined gravimetrically (Buschke et al., 2011) or calculated from OD_{660} values using the following correlation: $\text{CDM} [\text{g L}^{-1}] = 0.32 \times \text{OD}_{660}$ (Becker et al., 2009). Sugars and organic acids (glucose, trehalose, and glutarate) were quantified by HPLC (Agilent 1260 Infinity Series, Agilent Technologies, Waldbronn, Germany) using ion-moderated partition chromatography (Micro-guard cation cartridge, $30 \times 4.6 \text{ mm}$, Aminex HPX-87H, $300 \times 7.8 \text{ mm}$, Bio-Rad, Hercules, CA, USA) with $3.5 \text{ mM H}_2\text{SO}_4$ (55°C , 0.8 mL min^{-1}) as mobile phase. Detection was performed via refractive index, and external standards were used for quantification. Amino acids, including AVA, were quantified by HPLC (Agilent 1200 Series, Agilent Technologies) using α -aminobutyrate as internal standard and pre-column derivatization with *o*-phthalaldehyde and fluorenylmethylloxycarbonyl chloride (Rohles et al., 2016). The derivatized analytes were separated on a reversed phase column (Gemini 5 μm C18, $150 \times 4.6 \text{ mm}$, Phenomenex, Aschaffenburg, Germany) at 40°C and a flow rate of 1 mL min^{-1} using a gradient of $40 \text{ mM NaH}_2\text{PO}_4$ (0.5 g L^{-1} sodium azide, pH 7.8) and acetonitrile/methanol/water (45%/45%/10%), and detection was based on fluorescence measurement (340/450 nm).

2.8. Intracellular metabolite analysis

Cells were harvested by fast vacuum filtration ($0.2 \mu\text{m}$, Sartorius Stedim, Göttingen, Germany) and washed on the filter twice with 15 mL salt solution (2.5% NaCl) (Wittmann et al., 2004). For metabolite extraction, the filter was transferred into an aqueous solution (2 mL , $220 \mu\text{M}$ α -aminobutyrate, 100°C) and incubated in a water bath (100°C , 15 min). The obtained extract was clarified from debris ($8000\times\text{g}$, 5 min , 4°C). Afterwards, metabolites of interest were analyzed by HPLC, as described above. Experiments were conducted as biological triplicate.

2.9. Enzyme activity analysis

Cells were harvested, including a washing step (100 mM potassium phosphate buffer, pH 7.8). Subsequently, the suspension was transferred into lysing matrix B tubes (MP Biomedicals, OH, USA), followed by cell disruption (Precellys 24, Bertin Technologies, Ile de France, France). The obtained extract was clarified ($17,000\times\text{g}$, 4°C , 20 min). The reaction mixture (10 mL) for the analysis of DavA and DavB activity contained 22 mM L-lysine, 100 mM potassium phosphate buffer (pH 7.8), and $500 \mu\text{L}$ cell extract. Inhibitory effects of pathway intermediates on DavB activity were evaluated by the addition of AVA or L-lysine to the assay as given below. In all cases, the reaction mixture was incubated in baffled shake flasks (100 mL) on an orbital shaker (30°C , 230 rpm , HT Infors Multitron, Bottmingen, Switzerland). At different time points, samples were taken and immediately inactivated (100°C , 5 min , ThermoMixer, Eppendorf, Germany), followed by HPLC analysis of substrates and products. The activity of DavB was inferred from the consumption of L-lysine ($1 \text{ U} = 1 \mu\text{mol per minute}$), whereas the lumped production of AVA and glutarate was considered to derive the activity of DavA ($1 \text{ U} = 1 \mu\text{mol per minute}$). Specific activities were calculated on basis of the amount of protein in the cell extract (Becker et al., 2011). The assays were conducted as three biological replicates.

3. Results and discussion

3.1. *C. glutamicum* can grow in the presence of up to 140 g L^{-1} AVA

The major goal of this work was to enable *de novo* bio-based production of the carbon-5 platform chemical 5-aminovalerate on basis of the L-lysine-hyperproducing strain *C. glutamicum* LYS-12. LYS-12, previously upgraded from wild type by the implementation of twelve genomic modifications (Fig. 1), seemed a most straightforward host because it accumulated L-lysine, the AVA precursor, at a high yield of $0.55 \text{ g per gram of glucose}$, a titer of 120 g L^{-1} , and a productivity of $4.0 \text{ g L}^{-1} \text{ h}^{-1}$ (Becker et al., 2011). Moreover, it did not degrade L-lysine, but retained the amino acid inside the cell upon deletion of the lysine exporter *lysE* (Rohles et al., 2016), preventing loss of the precursor (Rohles et al., 2018).

C. glutamicum wild type was able to grow in the presence of up to 140 g L^{-1} AVA (1.2 M) (Fig. S1, Supplementary file 1). Increasing concentrations caused reduced growth rates, leading to a 50% growth reduction at an AVA concentration of 70 g L^{-1} . No growth was observed at 200 g L^{-1} AVA. *C. glutamicum* appeared significantly more tolerant to AVA than to related L-lysine-derived products like 1,5-diaminopentane (Kind et al., 2014) and glutarate (Rohles et al., 2018), both successfully produced at high level in the microbe before.

3.2. Genome-based monocistronic expression of native *davA* and *davB* under control of the *tuf* promoter is optimum for biosynthetic flux

Previous studies, using plasmids to express the *davBA* genes from *P. putida* for AVA production in *C. glutamicum*, revealed that the chosen genetic design has an influence on production performance (Park et al., 2014; Shin et al., 2016). Differently to these approaches, we aimed at fully genomic (plasmid-free) producers to enable optimum genetic stability and independence from the use of antibiotics. Therefore, our strategy was based on genomic expression of *davBA*. Given the mixed experience from previous work as discussed above, it appeared important to evaluate the genetic design. In addition to a previous layout that was based on monocistronic expression of the native genes *davBA* under control of the *tuf* promoter (P_{tuf}) (Rohles et al., 2016), we constructed two alternative pathway modules: a monocistronic, codon-optimized operon ($P_{tuf} \text{ } davBA^{opt}$) and a bicistronic variant ($P_{tuf} \text{ } davB \text{ } P_{tuf} \text{ } davA$) with native gene sequences, respectively. Hereby, codon optimization reduced the difference of the codon usage of *davB* and *davA* from that of highly expressed genes from 30% to 8% and from 30 to 9%, respectively (Fig. S2ABCD, Supplementary file 1).

To evaluate the impact of the three designs on the formation of AVA as well as its upstream and downstream side products, we tested them in *C. glutamicum* AVA-1. The basic producer excreted AVA, glutarate and L-

Table 2

Impact of the expression balance between *davA* and *davB* on the enzymatic capacity of the AVA pathway and the product spectrum in the basic producer *C. glutamicum* AVA-1 and derivatives with altered *davBA* expression pattern. All strains were grown on glucose minimal medium. The data represent the yields for AVA ($Y_{AVA/S}$), glutarate ($Y_{GTA/S}$), L-lysine ($Y_{Lys/S}$), and biomass ($Y_{X/S}$), and the specific enzymatic activities (EA) of DavB and DavA, related to the protein content. All strains exhibited similar specific growth rates in the range of $0.19 \pm 0.02 \text{ h}^{-1}$. The errors represent standard deviations from three biological replicates.

Strain	AVA-1 $P_{tuf} \text{ } davBA$	AVA-1 $P_{tuf} \text{ } davBA^{opt}$	AVA-1 $P_{tuf} \text{ } davB \text{ } P_{tuf} \text{ } davA$
$Y_{AVA/S} [\text{mmol mol}^{-1}]$	125.8 ± 4.2	99.4 ± 1.1	75.1 ± 6.2
$Y_{GTA/S} [\text{mmol mol}^{-1}]$	108.0 ± 9.1	55.3 ± 2.3	118.2 ± 5.6
$Y_{Lys/S} [\text{mmol mol}^{-1}]$	52.5 ± 3.3	58.7 ± 1.8	66.8 ± 2.8
$Y_{X/S} [\text{mmol g}^{-1}]$	51.8 ± 1.5	61.0 ± 3.3	39.3 ± 3.5
$EA_{DavA} (\text{mU mg}_{\text{Protein}}^{-1})$	1091 ± 14	28 ± 1	750 ± 30
$EA_{DavB} (\text{mU mg}_{\text{Protein}}^{-1})$	1036 ± 30	645 ± 25	949 ± 33

lysine, whereby AVA was the main product (Table 2). The monocistronic module with native genes, expressed in AVA-1, resulted in a high and well-balanced activity for DavA and DavB, above 1 U mg⁻¹ for each enzyme. The codon-optimized *davBA*^{opt} variant, however, revealed a strongly perturbed enzyme ratio. The activity of DavA was reduced by 97%, while that of DavB was reduced by 40%. The reduced capacity and the imbalance were obviously the reason for the strongly decreased production of AVA and glutarate and the enhanced secretion of L-lysine, upstream of the pathway (Table 2). Likewise, the bicistronic design with an extra promoter for *davA* expression was inferior in terms of AVA formation and catalytic activity, particularly regarding DavA (Table 2).

Previously, codon-optimization increased the expression of *ldcC* from *E. coli* in *C. glutamicum* (Kind et al., 2010). For *davBA* expression, however, codon-optimization yielded a mixed outcome (Park et al., 2014; Shin et al., 2016). The genes, previously enabling increased AVA production, were similarly codon-optimized as done here and their sequence differed similarly from the codon usage of highly expressed genes values (9% for *davB* and 9% *davA* (Shin et al., 2016) (Fig. S2EF, Supplementary file 1). Notably, *davAB* from the two donor strains *P. putida* KT2440 (this work) and *P. putida* ATCC 12633 (Shin et al., 2016), shared only 80% gene sequence homology, and the encoded proteins differed in the amino acid sequence (data not shown). Potentially this resulted in different secondary mRNA structures that could have influenced expression (Wan et al., 2011). Altogether, the monocistronic module with the native genes was selected as optimal for further work.

3.3. Streamlining of the catabolic GABA operon beneficially improves AVA production

Further strain engineering was based on *C. glutamicum* AVA-3 which carried the optimum genomic monocistronic *davBA* module. In a next step, we eliminated *gabD* (NCgl0463), annotated as succinate semialdehyde dehydrogenase, in AVA-3. The 1352 bp deletion was verified by a shortened PCR product (1069 bp versus 2421 bp for wild type) and confirmed by sequencing. The modification resulted in a double deletion of *gabD* and *gabT*, encoding catalytic conversions downstream of AVA (Fig. 1). The resulting strain AVA-4A, however, was not better. In fact, it produced 26% less AVA and 50% less glutarate than AVA-3 but grew faster and formed more biomass (Table 3). Next, we tackled *gabP* (NCgl0464), a GABA transporter chromosomally close to *gabT* (Zhao

Table 3

Growth and production performance of 5-aminovalerate producing *C. glutamicum* strains on glucose minimal medium. The analyzed strains comprise several derivatives of strain AVA-3, namely AVA-4A (AVA-3 Δ *gabD*), AVA-4B (AVA-3 Δ *gabP*), and AVA-4C (AVA-3 Δ *gabTDP*). Secretion of L-lysine was not observed in any of the strains due deletion of *lysE*. The data represent the yields for AVA ($Y_{AVA/S}$), glutarate ($Y_{GTA/S}$), and biomass ($Y_{X/S}$). Additionally, the specific rates of growth (μ), 5-aminovalerate production (q_{AVA}), glutarate production (q_{GTA}), and glucose uptake (q_{GLC}) are given. The data for the parent strain AVA-3 are taken from previous work (Rohles et al., 2016). The errors represent standard deviations from three biological replicates.

	AVA-3	AVA-4A	AVA-4B	AVA-4C
$Y_{AVA/S}$ [mmol mol ⁻¹]	274.9 ± 2.9	202.5 ± 3.0	278.2 ± 10.4	310.0 ± 3.7
$Y_{GTA/S}$ [mmol mol ⁻¹]	21.8 ± 1.4	10.7 ± 0.9	16.3 ± 0.0	10.6 ± 1.1
$Y_{X/S}$ [mmol g ⁻¹]	51.8 ± 0.5	64.0 ± 1.3	53.3 ± 2.8	47.6 ± 0.5
μ [h ⁻¹]	0.11 ± 0.00	0.14 ± 0.00	0.13 ± 0.00	0.11 ± 0.00
q_{AVA} [mmol g ⁻¹ h ⁻¹]	0.59 ± 0.02	0.45 ± 0.01	0.66 ± 0.06	0.73 ± 0.02
q_{GTA} [mmol g ⁻¹ h ⁻¹]	0.05 ± 0.05	0.02 ± 0.00	0.04 ± 0.00	0.02 ± 0.00
q_{GLC} [mmol g ⁻¹ h ⁻¹]	2.16 ± 0.07	2.21 ± 0.01	2.37 ± 0.13	2.37 ± 0.05

et al., 2012) Previously, *gabP* amplification increased the AVA re-import into *C. glutamicum* toward higher glutarate production (Rohles et al., 2018), supported by the structural similarity of GABA and AVA (Li et al., 2016). Here, we aimed to block the re-import of AVA by *gabP* and deleted 1190 bp of the gene in AVA-3. The genomic modification was verified by sequencing and a shortened PCR fragment of 1255 bp. The wild type, analyzed in comparison, yielded a fragment of 2445 bp. Strain AVA-4B (AVA-3 Δ *gabP*) revealed a slightly improved phenotype. The AVA production rate was increased by 20%, while the AVA yield remained constant. In addition, less glutarate was formed (Table 3).

Finally, the complete *gabTDP* operon was deleted. For this purpose, the plasmid pClik int *sacB* Δ *gabTDP* was transformed into *C. glutamicum* AVA-2 (the parent strain of AVA-3 that still contained *gabT*), yielding *C. glutamicum* AVA-4C. The desired mutant showed a PCR product of 1130 bp upon successful deletion, while a fragment of 5114 bp was found in case of wildtype colonies. The deletion of the entire *gabTDP* operon resulted in optimized production performance (Fig. 2AB). In shake flasks, strain AVA-4C produced AVA at a yield of 0.31 mol mol⁻¹ (0.2 g g⁻¹), 13% more than AVA-3 (Table 3). Among the different AVA-3 derivatives, it performed best. Beneficially, glutarate production was reduced by more than 50%, resulting in improved selectivity. The molar ratio between AVA and glutarate was increased from 12.6 (AVA-3) to 29.2 (AVA-4C), i. e. 2.3-fold. Obviously, the reduced AVA re-uptake complemented the beneficial effect of targeting intracellular AVA catabolism, underlining the power of synergistically optimizing transport and conversion in metabolic engineering (Kind et al., 2011a).

3.4. AVA massively accumulates inside the cells and poses a biosynthetic bottleneck

To get deeper insights into the AVA pathway, we characterized different producers from the strain genealogy for intracellular metabolites (Fig. 3). In particular, we were interested in the level of pathway intermediates inside the cells to identify the limiting steps (Kind et al., 2011b). In AVA-3 and AVA-4C, the intracellular level of L-lysine, upstream of the AVA pathway, was approximately 8 mM. Notably, this value was much lower than that observed for the parent L-lysine producer LYS-12, indicating that the introduced heterologous enzymes efficiently pulled L-lysine into the novel pathways. This effect was also reflected in reduced pools for L-aspartate and (to a weaker extent) L-alanine. However just as interesting, the intracellular L-lysine level of the AVA strains exceeded that of related cell factories, previously engineered to produce other derivatives of L-lysine (Buschke et al., 2013). As example, cells of the diaminovalerate producer *C. glutamicum* DAP-3C, expressing L-lysine decarboxylase to enable production of the diamine from L-lysine, contained 4-fold less L-lysine (Kind et al., 2011b). Like the AVA strain family in this work, the DAP-3C mutant had been previously upgraded from the same L-lysine overproducer LYS-12 (Becker et al., 2011). Due to this, the genetic background, except for the individual heterologous pathways, was identical. The higher accumulation of L-lysine in the AVA strains therefore pointed to a bottleneck in the terminal product pathway, either in AVA formation or export. The pool of the L-lysine precursor L-aspartate, further upstream in metabolism, and that of amino acids from other pathways (Fig. 3), was comparable in AVA and diaminovalerate producers (Kind et al., 2011b), respectively, indicating that the bottleneck was located around the AVA pathway. A big surprise, then, was the intracellular level of AVA itself. The product was contained in enormous quantities inside the cells. Strains AVA-3 and AVA-4C accumulated 340 mM of intracellular AVA. By comparison, the level of intracellular diaminovalerate in corresponding producers was only 10 mM, more than 30-fold lower (Kind et al., 2011b). Interestingly, AVA was 42-fold in excess relative to L-lysine (Fig. 3A). Because DavB was known to be influenced by other pathway intermediates (Vandecasteele and Hermann, 1972), we evaluated the impact of increased levels of L-lysine and AVA on the activity of the enzyme (Fig. 4A). At L-lysine concentrations above 25 mM, the

activity of DavB was slightly reduced. However, this inhibition seemed to play no significant role during production, given that the intracellular level of L-lysine *in vivo* was below this value (Fig. 3). In contrast, the inhibition by AVA appeared relevant, as the enzyme was negatively affected at AVA levels far below the intracellular amount (Fig. 4B). This might explain, why DavB operated below 0.5% of its available capacity, when comparing *in vitro* capacity and *in vivo* flux. Exemplified for AVA-3, the activity of DavB found *in vitro* ($2072 \text{ mU mg}_{\text{CDM}}^{-1}$, considering a protein content of 50%) represented a maximum possible flux capacity of $131 \text{ mmol g}^{-1} \text{ h}^{-1}$ for the AVA pathway. This value was 222-fold higher than the real flux of $0.59 \text{ mmol g}^{-1} \text{ h}^{-1}$ (Table 3).

Altogether, several important findings were made by metabolite and enzyme analysis. First, AVA export was found to severely limit production. Although all AVA-producers successfully excreted the product, they did not provide sufficient transport capacity to meet the incoming flux so that a large fraction of the product remained inside. This situation also explained the significant benefit of eliminating the AVA re-import. Second, driven by the high activity of DavA and DavB, the AVA pathway still managed to convert 95% of the intracellular L-lysine into AVA. However, the high intracellular AVA level prevented a higher flux due to the feedback inhibition of DavB (Vandecasteele and Hermann, 1972).

3.5. Three native GABA permease-like transporters do not offer potential for strain improvement

Given the massive accumulation of AVA inside the cells, the export of the product was tackled next. First, we explored native transporters of *C. glutamicum*. GabP is supposed to be the major GABA transporter in the microbe (Zhao et al., 2012). However, as shown, the protein worked as importer (Fig. 2AB) (Rohles et al., 2018) so that other transporters had to mediate AVA secretion. To date, these are not known (Perez-Garcia and Wendisch, 2018). GABA permeases from other bacteria, also named GabP, share a low sequence identity with the specific GabP transporter from *C. glutamicum* (Dagorn et al., 2013). They are found in different pseudomonads such as *P. putida*, *P. syringae* (McCraw et al., 2016), *P. aeruginosa* (NOE and Nickerson, 1958), *P. fluorescens* (Tunnickliff, 1993), and also *E. coli* (Richard and Foster, 2003). Differently to *C. glutamicum*, these microbes not only metabolize but also synthesize and excrete GABA.

Because GABA permeases also act on the structural homologue AVA, they displayed an interesting blueprint. We selected GabP-III (PP2911), one out of five GABA transporters of *P. putida* KT2440 as template (dos Santos et al., 2004). This microbe appeared as a suitable donor due to the efficient expression of its *davBA* genes in *C. glutamicum*. Furthermore, GabP-III had been functionally expressed in *E. coli* indicating that this membrane protein works in heterologous hosts (Li et al., 2016). Using the amino acid sequence of GabP-III, we searched for homologues in the genome of *C. glutamicum*. The protein-based BLAST identified three membrane proteins with high E-value (Table S2, supplementary file 1): PheP, assigned as transporter for L-phenylalanine (Zhao et al., 2011) and AroP, a transporter for L-histidine and aromatic amino acids (Shang et al., 2013). Both proteins, however, have not been tested for GABA or AVA before. CycA was a putative D-serine, D-alanine, and glycine transporter (Schneider et al., 2004), potentially of interest because some GABA permeases also accept L-serine as a substrate (Pavic et al., 2021). Therefore, each of the three encoding genes was individually deleted from the genome of AVA-producing *C. glutamicum*.

None of the deletion mutants, however, exhibited significantly reduced AVA secretion (Fig. S3, supplementary file 1). One of them slightly secreted even more AVA, eventually because less glutarate was made. It therefore remained open, which of the native membrane protein(s) enabled AVA excretion in the overproducers, requiring more work in the future (Perez-Garcia and Wendisch, 2018). Regarding superior production, the three native candidates did not prove to be suitable targets, so that heterologous transport proteins became the focus for further optimization.

3.6. Heterologous expression of the GABA III permease from *P. putida* KT2440 increases AVA export

In a next step, heterologous permeases were tested. *P. putida* KT2440 encodes five transporters for GABA (PP4106, PP2911, PP4756, PP2543, and PP0284) (dos Santos et al., 2004). We considered GabP-III (PP2911) as promising candidate, given the reasons above. A copy of GabP-III, preceded by P_{uvf} and a ribosomal binding site of *C. glutamicum*, was integrated at the deleted *gabTDP* site of *C. glutamicum* AVA-4C, which yielded *C. glutamicum* AVA-5A. The novel mutant AVA-5A accumulated more than 20 mM AVA with slight amounts of glutarate (Fig. 2 CD). Its AVA yield ($0.36 \text{ mol mol}^{-1}$) and specific AVA production rate ($0.87 \text{ mmol g}^{-1} \text{ h}^{-1}$) were increased by 17% and 19%, as compared to AVA-4C (Table 3, Table 4). This proved functional expression of the membrane protein in *C. glutamicum*. Furthermore, GabP-III beneficially uncorked the bottleneck at the level product export. In *P. putida* KT2440, the transport protein is described as importer for GABA, contributing to GABA catabolism (dos Santos et al., 2004). In *C. glutamicum* AVA-5A, however, it acted as exporter. Exporting AVA activity of GabP-III was also observed before (Liu et al., 2014). This reversal in transport was likely driven by the immense concentration of AVA inside the cells (Fig. 3). The newly installed transporter, however, did not reduce glutarate formation. The five-carbon diacid remained as by-product. AVA-5A formed less biomass than its predecessor, related to the larger fraction of carbon which was reallocated for AVA formation (Table 3, Table 4). In terms of AVA yield, AVA-5A surpassed all previous strain engineering efforts (Cheng et al., 2021) and, based on shake flask cultures, even reached the performance of high-yield *C. glutamicum* strains for other products (Becker et al., 2011; Hoffmann et al., 2018; Kind et al., 2014; Rohles et al., 2018). Given the positive effect of GabP-III on performance and the still high intracellular AVA pool, a next round of strain engineering aimed to further enhance the export capacity. To this end, strain AVA-5A was upgraded by expressing a second copy of GabP-III, again preceded by P_{uvf} and a ribosomal binding site of *C. glutamicum* in the *crtI2* locus (encoding for a step of carotenoid biosynthesis). The new mutant, AVA-5B, exhibited a slightly higher AVA yield (Table 4), but grew slower, exhibited a slightly increased intracellular AVA level (Fig. 3), and also formed a bit more glutarate. The increased AVA yield was clearly beneficial, but the side effects were disadvantageous. It seemed that the expression of the transporter in strain AVA-5B was eventually too strong. Likewise, high-level expression of membrane proteins caused negatively affected the vitality of *C. glutamicum* cell factories in a previous study (Kind et al., 2011b). Altogether, transporter expression from a single genomic gene copy seemed optimal at this stage.

3.7. *C. glutamicum* AVA-5A produces more than 48 g L^{-1} of AVA but runs into low selectivity at high titers

To assess performance under industrially relevant conditions, we benchmarked the AVA-5A strain in a fed-batch process on a glucose medium (Fig. 5A). During the batch phase, the strain grew exponentially and accumulated AVA at a yield of $0.35 \text{ mol mol}^{-1}$ (0.23 g g^{-1}). In this way, *C. glutamicum* handled the high start concentration of the sugar (80 g L^{-1}) well. After 28 h, the initially supplied glucose was depleted, and the feed phase was started. Pulses of the concentrated feed were automatically added, when the sugar was exhausted, which was nicely reflected by a sudden increase of the DO level. This correlation allowed precise control. Previous fermentations with *C. glutamicum* have shown that the microbe also performs well with other feed regimes such as linear ramps and pulse-wise additions, manually controlled using at-line monitoring of the sugar level (Kind et al., 2014). The DO-based control chosen here, however, appears particularly robust and does not need external monitoring (Rohles et al., 2018). After 40 h, the maximum biomass concentration (51.6 g L^{-1}) was reached. The AVA level continuously increased from 17.4 g L^{-1} at the end of the batch phase to a

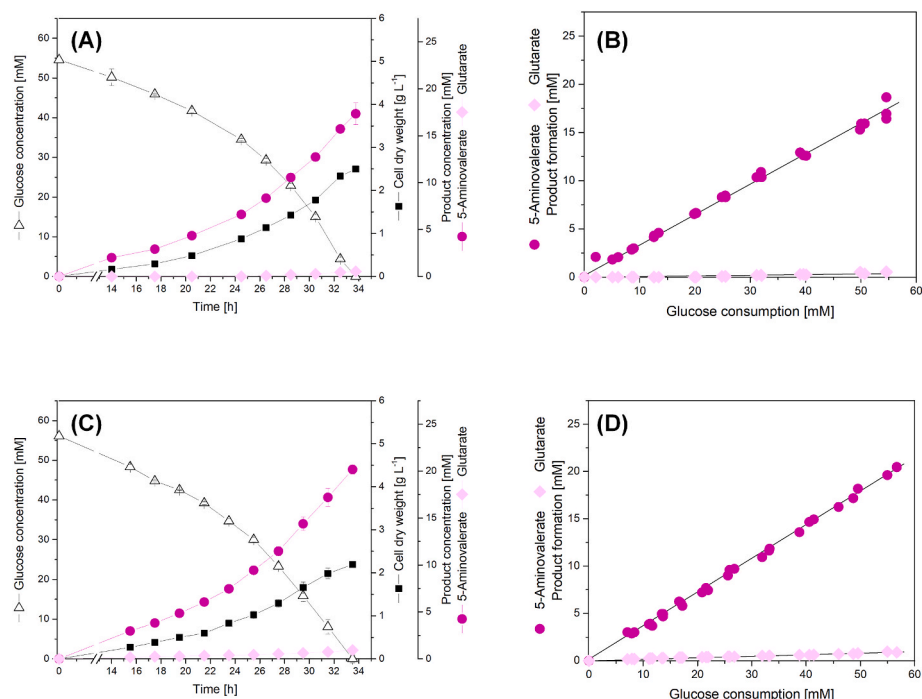


Fig. 2. Growth and production characteristics of basic 5-aminovalerate (AVA) producing *C. glutamicum* strains. The strains AVA-4C (A, B) and AVA-5A (C, D) were cultivated in shake flasks at 30 °C in a chemically defined glucose medium. The cultivation profiles show growth, product and by-product formation, and glucose consumption over time (A, C), and corresponding yields (B, D). Error bars represent standard deviations from three biological replicates.

final titer of 48.3 g L⁻¹ (411 mM) after 96 h, the highest value reported so far for *de novo* production of AVA and an attractive feature of the strain (Cheng et al., 2021). Unfavorably, glutarate strongly accumulated during the feed-phase. The final glutarate level was 7 g L⁻¹. Overall, 15% of intracellular AVA was therefore metabolized undesirably. The AVA yield, based on consumed glucose, was surprisingly reduced during the feed phase (0.33 mol mol⁻¹). Although it still exceeded the state-of-art by 65% (Cheng et al., 2021), there seemed space for improvement. *C. glutamicum* cell factories can achieve substantially increased product yields during the feed phase (Becker et al., 2011; Kind et al., 2014; Rohles et al., 2018). The space-time yield for AVA was maximal during the feed phase (0.77 g L⁻¹ h⁻¹). Averaged over the full process, production occurred at more than the half-maximum rate (0.50 g L⁻¹ h⁻¹).

An important observation emerged when inspecting the selectivity of the process over time (Fig. 5B). The ratio between newly formed AVA and glutarate became more and more unfavorable, the longer the process was operated. During the early stage, the relative amount of glutarate produced was below 3–5% of the amount of AVA formed. However, this picture drastically changed. In later phases of the process the relative glutarate formation increased to 30%, indicating that cells had largely lost their selectivity. The continuous loss of selectivity over time (eventually even worsening at higher AVA levels) has dramatic consequences for the design of industrial AVA production strains. Glutarate accumulation would become a performance killer when aiming for AVA titers of 80 g L⁻¹ and above, required for economic viability for such type of products (van Duuren et al., 2020). An attractive process at high titer and selectivity appeared not feasible without the complete elimination of glutarate formation.

3.8. Discovery of a second AVA transaminase in the *L*-arginine biosynthetic pathway

As shown, *C. glutamicum* AVA-5A and AVA-5B still formed glutarate as by-product, preventing selective AVA production at high-level (Fig. 5AB). *C. glutamicum* enzymes that degrade AVA in addition to

GabT were not known but now emerged as crucial targets for strain improvement. We hypothesized that the unfavorable activity was due to enzyme promiscuity and that the microbe possessed one or more other enzymes that accepted AVA, in addition to their natural substrate. Since the GabT protein from *C. glutamicum* showed such nonspecificity, we used its structure as a blueprint to identify potential candidates. GabT belonged to the family of pyridoxal phosphate-dependent aminotransferases of class III that are characterized by specific structural motives to bind the cofactor and transfer the amino group of the substrate onto 2-oxoacids (Hong and Kim, 2019). A protein-protein BLAST of GabT against the genome of *C. glutamicum* ATCC 13032 yielded 4 candidates with high similarity (Table S3, supplementary file 1).

In *C. glutamicum*, ArgD (N-acetyl-ornithine transaminase), catalyzes the amination of N-acetyl-L-glutamate semialdehyde into N-acetyl-L-ornithine during *L*-arginine biosynthesis from *L*-glutamate. Experimental analysis of ArgD from *C. glutamicum* had revealed no other function (Marienhagen et al., 2005).

Anyway, we deleted *argD* in strain AVA-3 to evaluate its potential role. Using the integrative plasmid pClik int *sacB* Δ *argD*, the designated mutant AVA-6A was constructed and verified by sequencing and its truncated PCR fragment of 1120 bp versus 2295 bp in wild type. The Δ *argD* strain could no longer grow in minimal medium without *L*-arginine, as expected (data not shown). Advantageously, genomic deletion of *argD* completely abolished glutarate formation (Table 4). The by-product was no longer detectable.

This observation proved that ArgD, in addition to its native role in *L*-arginine biosynthesis, exhibited AVA transaminase activity. Favorably, the AVA yield in the novel strain was increased by 41% to 0.44 mol mol⁻¹. The AVA productivity was even increased by 57%. The new producer AVA-6A, supplemented with a small amount of yeast extract to compensate for the auxotrophy, grew similar to strains that were not supplemented (Table 3, Table 4), indicating that the improved performance was specifically caused by the genomic modification and not a general growth benefit.

ArgD was the only enzyme in *C. glutamicum* (in addition to GabT) that contributed to AVA loss. The deletion of NCgl2335 in AVA-3, done

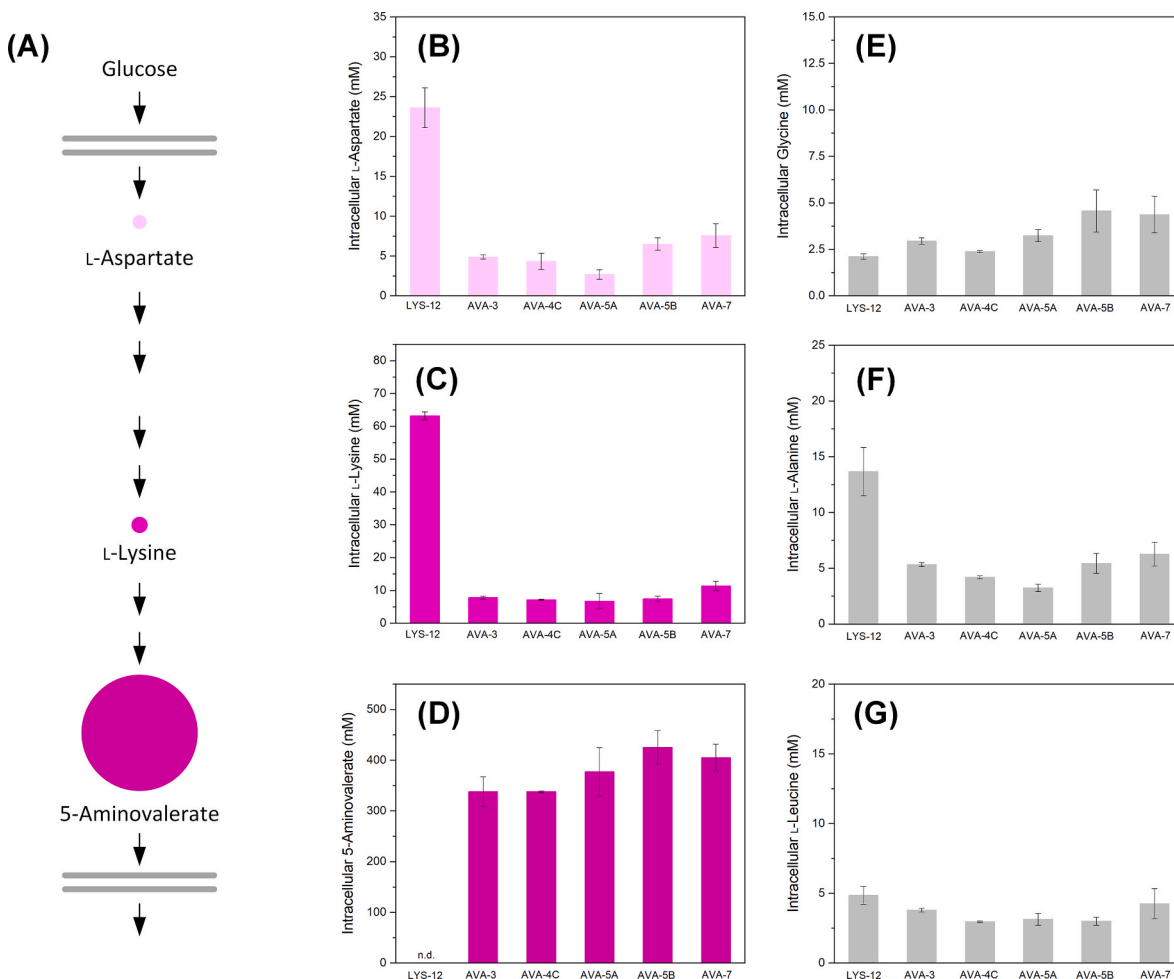


Fig. 3. Metabolic profiling of 5-aminovaleate (AVA) producing *C. glutamicum* strains AVA-3, AVA-4C, AVA-5A, AVA-5B, and AVA-7 and the parent *l*-lysine producing strain LYS-12. The microbes were grown in shake flasks at 30 °C on a medium with 10g L⁻¹ glucose, whereby strain AVA-7 was additionally supplemented with yeast extract (1.5 g L⁻¹). The intracellular levels of different amino acids and AVA were quantified during the mid-production phase. The given concentrations were inferred from the estimated analyte amount per sampled cell dry mass (CDM), considering a cell volume of 1.95 μL mg_{CDM}⁻¹ (Krömer et al., 2004). In addition for strain AVA-4C, the pool sizes are visualized as circles, whereby the differences are proportional to the displayed areas (Gläser et al., 2020). Error bars represent standard deviations from three biological replicates.

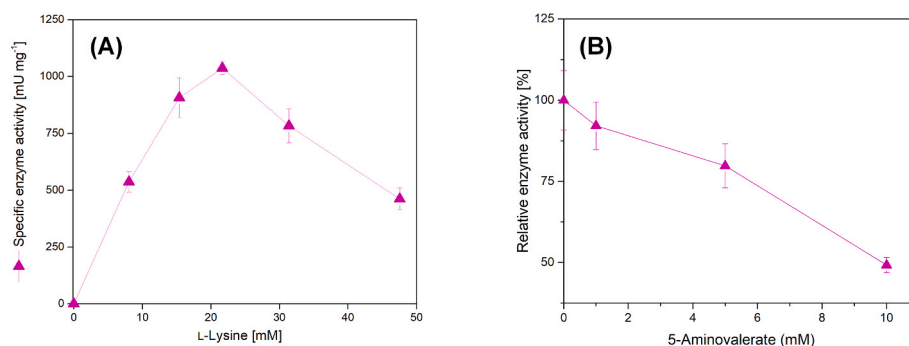


Fig. 4. Kinetic analysis of *l*-lysine monooxygenase (DavB) from *P. putida* KT2440, expressed in *C. glutamicum* AVA-1 for 5-aminovaleate (AVA) production. The microbe was grown in shake flasks at 30 °C on minimal glucose medium. The enzymatic activity was assessed during the mid-production phase. Error bars represent standard deviations from three biological replicates.

in parallel and verified by PCR (1101 bp versus 2471 bp fragment size) and sequencing, did not yield a phenotype (data not shown). The two remaining candidates, NCgl2515 and NCgl0422 were regarded insignificant and not explored further. NCgl2515 had previously shown very weak activity for GABA (Shi et al., 2017). We cannot not exclude from our data that this enzyme might accept also AVA, but if at all such

activity exists, it did not play a role here.

Several important conclusions could be drawn. So far undiscovered, ArgD exhibited AVA transaminase activity. It was the only enzyme remaining that caused the undesired glutarate formation. Therefore, *argD* displayed a crucial target toward improved AVA production. In catalyzing the deamination of AVA, ArgD, interestingly, worked in the

Table 4

Selective AVA production in advanced *C. glutamicum* cell factories. The analyzed strains comprise AVA-5A, AVA-6A, AVA-6B, AVA-7, and AVA-8. The data represent the yields for 5-aminovalerate ($Y_{AVA/S}$), glutarate ($Y_{GTA/S}$), and biomass ($Y_{X/S}$). Additionally, the specific rates of growth (μ), 5-aminovalerate production (q_{AVA}), glutarate production (q_{GTA}), and glucose uptake (q_{GLC}) are given. Secretion of L-lysine was not observed due to the deletion of *lysE* in all strains. The given errors represent standard deviations from three biological replicates. AVA-5A and AVA-5B were grown on minimal glucose medium. The medium of the other strains was additionally supplemented with 1.5 g L⁻¹ yeast extract to account for the implemented L-arginine auxotrophy. Accordingly, the yield calculation for these strains considered glucose and additionally measured free amino acids from the yeast extract (data not shown). The latter contributed approximately 7% extra carbon. For simplicity, 1 mol of each amino acid was counted as one mol of glucose, providing a restrained yield estimate, due to the lower number of carbons in amino acids than in the sugar.

	AVA-5A	AVA-5B	AVA-6A	AVA-6B	AVA-7	AVA-8
$Y_{AVA/S}$ [mmol mol ⁻¹]	361.6 ± 2.9	382.1 ± 0.0	438.5 ± 22.2	441.5 ± 5.7	557.3 ± 26.6	532.4 ± 8.3
$Y_{GTA/S}$ [mmol mol ⁻¹]	13.5 ± 0.3	15.1 ± 0.2	n.d. ^a	n.d. ^a	n.d. ^a	n.d. ^a
$Y_{X/S}$ [mmol g ⁻¹]	42.7 ± 1.9	35.8 ± 3.2	41.4 ± 1.8	38.4 ± 2.0	31.3 ± 1.5	42.5 ± 1.5
μ [h ⁻¹]	0.10 ± 0.00	0.08 ± 0.00	0.10 ± 0.01	0.10 ± 0.00	0.10 ± 0.00	0.09 ± 0.00
q_{AVA} [mmol g ⁻¹ h ⁻¹]	0.87 ± 0.01	0.91 ± 0.01	1.16 ± 0.12	1.15 ± 0.02	1.74 ± 0.05	1.61 ± 0.05
q_{GTA} [mmol g ⁻¹ h ⁻¹]	0.03 ± 0.00	0.03 ± 0.00	n.d. ^a	n.d. ^a	n.d. ^a	n.d. ^a
q_{GLC} [mmol g ⁻¹ h ⁻¹]	2.41 ± 0.03	2.36 ± 0.02	2.65 ± 0.16	2.60 ± 0.05	3.12 ± 0.19	2.67 ± 0.16

^a n.d. = not detectable.

opposite direction than in L-arginine biosynthesis, where it aminates N-acetyl-glutamate-5-semialdehyde. The reversal operation was likely driven by the high intracellular AVA availability (Fig. 3).

3.9. *C. glutamicum* AVA-6A benefits from a range of L-arginine-containing supplements to produce AVA

Different supplements were tested to find a suitable medium for *C. glutamicum* AVA-6A that compensated for the introduced L-arginine auxotrophy. A miniaturized culture system with 48 well plates was used for this purpose. AVA-6A grew with all tested supplements, L-arginine, casamino acids, and yeast extract, respectively, and produced AVA in all cases (Fig. S4, supplementary file 1). When adding pure L-arginine, growth was somewhat reduced, but AVA formation was highest. Casamino acids, and yeast extract enabled better growth. Higher amounts of each supplement increased the specific growth rate and slightly reduced the AVA yield, indicating a competition for carbon between cell growth and product formation, as observed before in *C. glutamicum* for other products (Becker et al., 2011). Out of all combinations, yeast extract, added at a level of 1.5 g L⁻¹, provided a good balance between growth and product formation. This condition was therefore kept for further cultivations.

In next step, the beneficial modifications $\Delta argD$ and $\Delta gabDTP$ were combined in one strain. For this purpose, *argD* was removed from strain AVA-4C, including verification by PCR and sequencing. The new strain, designated *C. glutamicum* AVA-6B, was evaluated (Fig. 6AB). Different to its parent strain AVA-4C which was continuously growing until glucose was depleted, AVA-6B showed a two-phase behavior. Likely becoming L-arginine-limited, the mutant stopped growth after 24 h while glucose was still available. However, it continued to take up the sugar and fully depleted glucose within 36 h. Over the whole culture time, AVA was

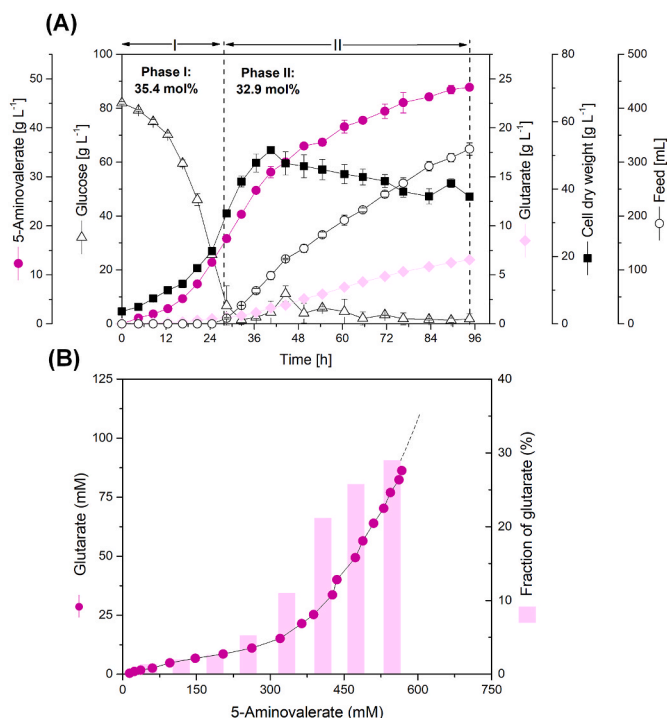


Fig. 5. Fed-batch production of 5-aminovalerate (AVA) by metabolically engineered *C. glutamicum* AVA-5A: culture profile (A) and product selectivity over time (B). After depletion of the initial sugar, pulses of feed were added automatically, using an increase of the level of dissolved oxygen (DO) above 45% as a trigger. Regarding the culture profile, batch and feed phase are denoted by a dotted line, and the average AVA yield for each phase is indicated. The batch medium contained glucose (80 g L⁻¹) and yeast extract (15 g L⁻¹) as carbon source. In the feed, the level of glucose (600 g L⁻¹) was 7.5-fold increased, while the yeast extract level (15 g L⁻¹) remained the same. Regarding product selectivity, the data show the accumulation of the desired product AVA versus that of the undesired by-product glutarate along the process (B). In addition, the relative abundance of newly formed glutarate at different stages of the process is shown as fraction of newly formed total product (glutarate plus AVA). The data represent mean values and deviations from two replicates.

accumulated in a linear manner to a final level of 24 mM, 60% more than for AVA-4C. The AVA yield was as high as 0.44 mol mol⁻¹. Notably, less carbon was used for anabolism by AVA-6B (Table 4). Overall, the introduced auxotrophy, supported by small amounts of yeast extract, enabled an efficient mode of decoupled growth and product formation.

3.10. *C. glutamicum* AVA-7 shows highly selective AVA production without by-products

Finally, all beneficial targets were assembled in one strain. For this purpose, PP2911 was cloned into strain AVA-6B. The new producer *C. glutamicum* AVA-7 comprised all beneficial modifications. In batch-mode, AVA-7 formed 25 mM AVA (Fig. 6CD) and achieved an AVA yield of 0.56 mol mol⁻¹, even 26% more than AVA-6B (Table 4). The yield corresponded to 74% of the theoretical maximum yield (Becker et al., 2011), demonstrating high synthetic capability of the new cell factory. Notably, the L-lysine-yield of the parent L-lysine-producer LYS-12, used to create AVA-7, was only 0.26 mol mol⁻¹, when determined under similar conditions (Becker et al., 2011). AVA-7 surpassed this value by 215%. This leap in performance impressively underlines how much extra carbon could be pushed and pulled through L-lysine biosynthesis towards the novel product. The integration of a second gene copy into AVA-7 encoding the AVA exporter GABA-III, provided strain AVA-8. The additional modification, however, did not yield further

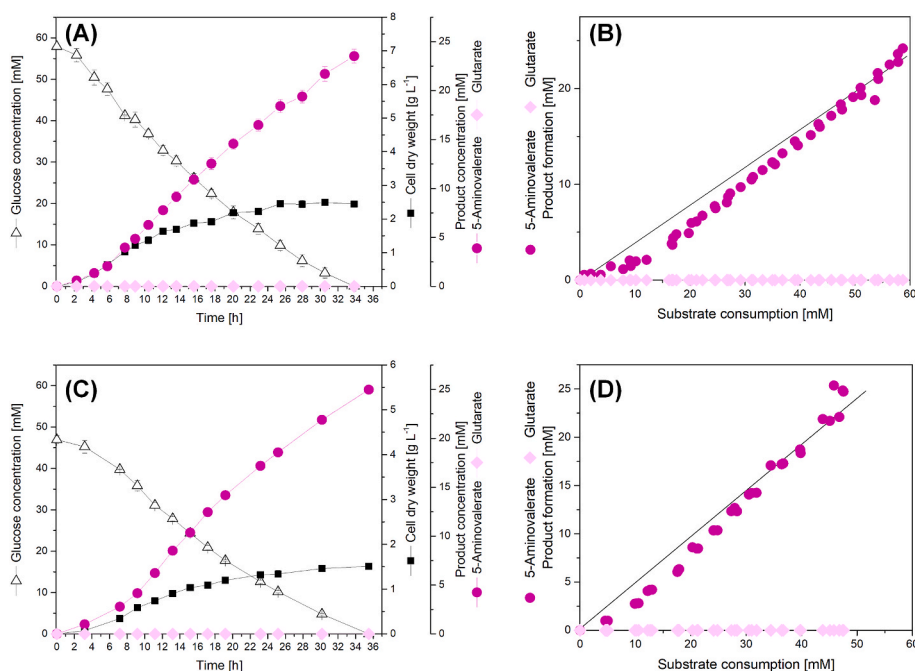


Fig. 6. Growth and production characteristics of advanced 5-aminovaleate (AVA) producing *C. glutamicum* strains. The strains AVA-6B (A, B) and AVA-7 (C, D) were cultivated in shake flasks at 30 °C. The medium contained glucose (10 g L⁻¹) as major carbon source and was additionally amended with yeast extract (1.5 g L⁻¹). The cultivation profiles show growth, product and by-product formation, and glucose consumption over time (A, C), and corresponding yields (B, D). Error bars represent standard deviations from three biological replicates.

improvement but was rather detrimental (Table 4) so that strain AVA-7 emerged as the best producer.

AVA-7 was now evaluated in a glucose-based fed-batch process (Fig. 7). Favorably, AVA production was enhanced already during the batch phase and reached a level of 20.5 g L⁻¹ after 28 h (20% more than AVA-5A). Regarding growth, AVA-7 efficiently utilized glucose right from the start and, like AVA-5A, achieved a cell concentration of 31.9 g L⁻¹ during the batch phase which lasted 28 h. The similarity in growth indicated that the supplements initially added, compensated for the deletion of *argD*. However, with the entry into the feed phase, growth flattened off much more strongly for AVA-7. The maximum biomass concentration (37.3 g L⁻¹) after 36 h was almost 30% lower than for AVA-5A. Further on, the production of AVA was kept high and reached 46.5 g L⁻¹ (396 mM) after 76 h. Notably, the cells required much less glucose during the feed phase, and a high yield of 0.52 mol mol⁻¹ (0.34 g g⁻¹) was achieved (Fig. 7). Although a slight overestimation cannot be excluded, due to small amounts of yeast extract added (below 3/100 of sugar in feed), the created cell factory exhibited an attractive synthetic selectivity.

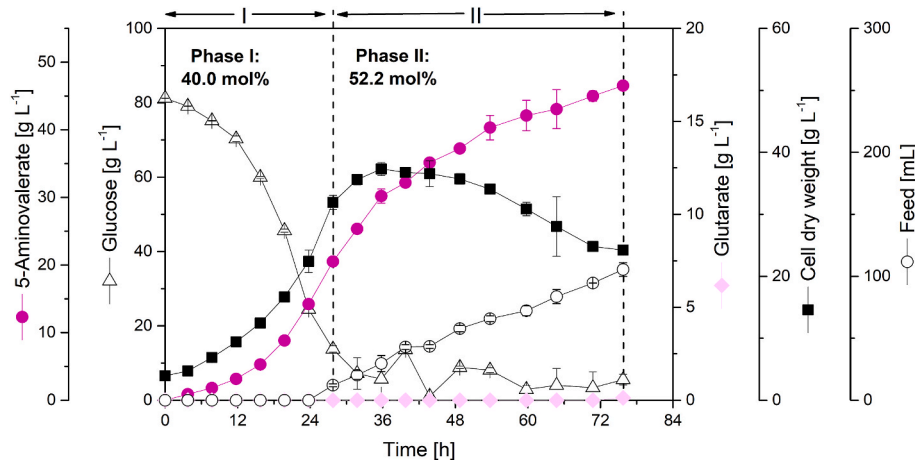


Fig. 7. Fed-batch production of 5-aminovaleate (AVA) by metabolically engineered *C. glutamicum* AVA-7. After depletion of the initial sugar at the end of the batch phase, pulses of feed were added automatically, using an increase of the level of dissolved oxygen (DO) above 45% as a trigger. Regarding the culture profile, batch and feed phase are denoted by a dotted line, and the average AVA yield for each phase is indicated. The batch medium contained glucose (80 g L⁻¹) and yeast extract (15 g L⁻¹) as carbon source. In the feed, the level of glucose (600 g L⁻¹) was 7.5-fold increased, while the yeast extract level (15 g L⁻¹) remained the same. The data represent mean values and deviations from two replicates.

4. Conclusions

The developed strains of *C. glutamicum* display valuable hosts for industrial AVA production.

They are feasible to provide AVA from renewable resources and are applicable to production in technical scale. As shown, they outperform all reported microbes, previously engineered for AVA *de novo* production in the key performance indicators yield, titer and rate (Fig. 8). Notably, the novel cell factories are genome-based and genetically fully defined, offer high genetic stability and (not relying on plasmids) enable to dispense with the use of antibiotic selection markers. The high performance was achieved by step-wise systems metabolic engineering which provided a set of synergistically acting beneficial genomic modifications at the level of precursor supply, AVA biosynthesis, AVA transport into and out of the cell, and undesired AVA withdrawal. For the first time, by-product formation could be fully abolished. Given the fact, that production costs for large scale chemicals ultimately rise and fall with selectivity and yield, the development of strains AVA-6B and AVA-7 is a milestone towards industrial manufacturing of AVA using *de novo* fermentation from sugar and opens up a great portfolio of opportunities.

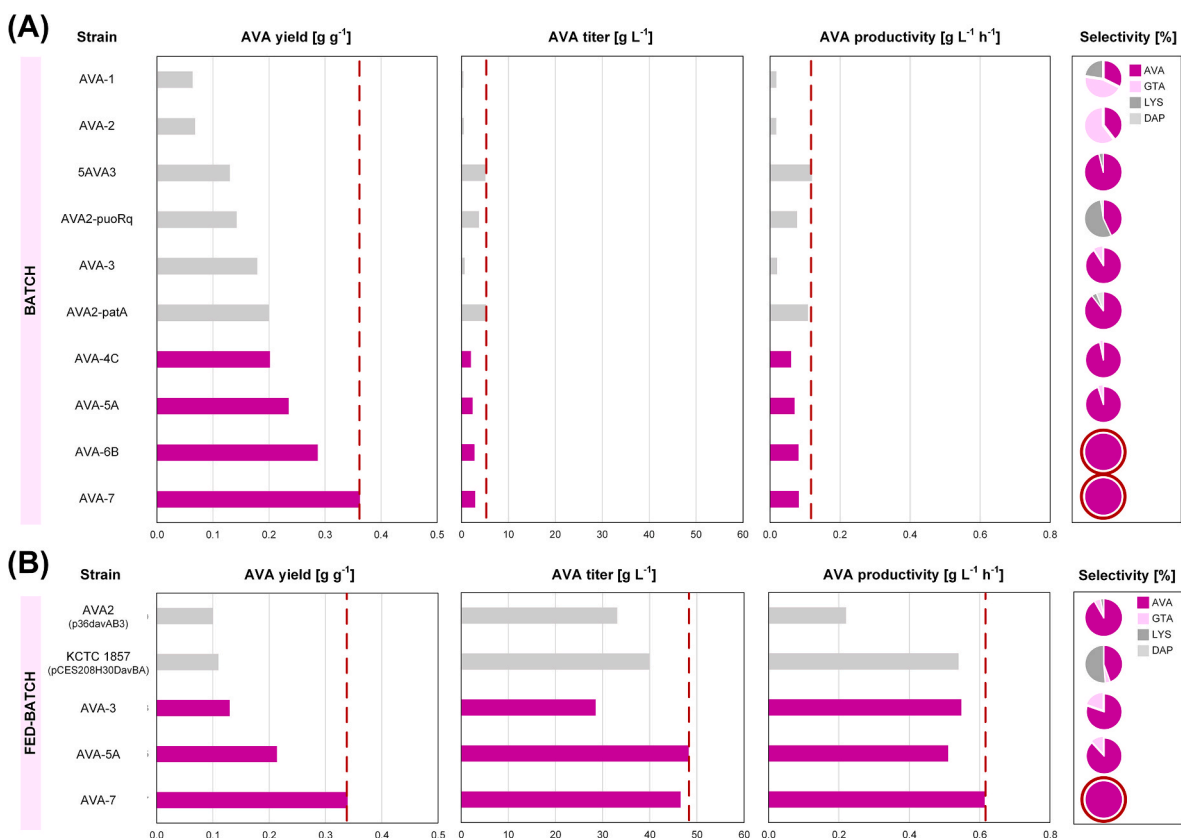


Fig. 8. Benchmark of microbial de-novo 5-aminovaleate production. The different developments are evaluated and compared based on titer, rate, yield, and selectivity. Both, batch and fed-batch production processes are displayed. For each criterion, the achieved optimum is indicated by a dashed line. AVA, 5-aminovaleate; GTA, glutarate; LYS, L-lysine; DAP, diaminopentane. A red circle around the products indicates exclusive formation of AVA. Different cell factories were used for AVA production, including *C. glutamicum* AVA-1 and AVA-2 (Rohles et al., 2016), *C. glutamicum* AVA-3, AVA-4C, AVA-5A, AVA-6B, and AVA-7 (this work), *C. glutamicum* 5-AVA3 (Jorge et al., 2017), *C. glutamicum* AVA2 p36 *davAB3* (Shin et al., 2016), *C. glutamicum* KCTC 1857 pCES208H30 *davBA* (Joo et al., 2017), as well as *C. glutamicum* AVA2-*puoRq* and AVA2-*patA* (Hauptka et al., 2020).

The discovery of the coupling between AVA metabolism and L-arginine biosynthesis toward deleting the *argD* gene for full selectivity is a major finding of this work and should deserve a few final conclusions (Fig. S5, supplementary file 1): (i) from a structural perspective, AVA and N-acetyl-ornithine (the native substrate of ArgD) both possess a linear 5 carbon chain with a terminal amino/aldehyde group that undergoes (de)amination, while AVA is smaller, lacking the sterically voluminous N-acetyl-residue. This similarity obviously provided sufficient affinity for AVA to be accepted by the enzyme; (ii) from an engineering perspective, the discovery of ArgD is an excellent example for the challenges related to translation and upscaling. The formation of glutarate as by-product was minor in batch processes and appeared somewhat tolerable, whereas fed-batch production suddenly ran into unexpected substantial glutarate accumulation and poor selectivity at high titer. This problem presumably occurs in any AVA producing *C. glutamicum*, independent of the biosynthetic route, and it would be interesting to study this effect in related biotransformations that produce AVA from L-lysine; (iii) from a process perspective, the pronounced accumulation of glutarate in later process phases could be due to two reasons. First, the cell factories exhibited reduced and finally no more growth during production, something which is typical for industrial fermentation processes, where producing strains are intentionally driven into growth limitation to support product build-up (Becker and Wittmann, 2012; Eggeling and Bott, 2015; Graf et al., 2018). The halted growth, however, made ArgD unbusy. Because biosynthetic pathways are shut off in such a condition, the enzyme likely more and more lacked its native substrate N-acetyl-ornithine and, *inter alia*, was free to convert AVA at high rate instead (Fig. S5, supplementary file 1). Second,

increasing titers of extracellular AVA and the built-up of an unfavorable concentration gradient could have hampered export, triggering higher intracellular accumulation and an even stronger push of AVA down the pathway to glutarate. More work is needed in the future to resolve this fascinating picture. In any case, the deletion of ArgD killed two birds with one stone: it allowed to control growth much better, while directing carbon from anabolism and by-product pathways to product formation, resulting in high yield. Engineering of ArgD on the protein level or dynamic control of its expression could help to eliminate its undesired promiscuity either completely or during later process stages. Eventually, this could enable AVA production without supplements that were added here to overcome the introduced arginine-auxotrophy.

Regarding other hosts for AVA production, the ArgD protein of *C. glutamicum* differs from ArgD in *E. coli* which exhibits both N-acetyl-ornithine and N-succinyl-L,L-diaminopimelate aminotransferase activities with a very similar catalytic efficiency and identical kinetic mechanism (Fondi et al., 2007). In *C. glutamicum*, the latter conversion is catalyzed by DapC instead, specifically separating the biosynthetic routes of L-arginine and L-lysine (Hartmann et al., 2003). In *E. coli*, deletion of ArgD, as successfully used here, would block the formation of L-lysine, upstream of AVA and saw-off the branch of precursor supply. Extensive engineering would be needed to bypass this problem, suggesting *C. glutamicum* as superior host for bio-based AVA production at this stage.

Author statement

Christina Rohles, Sarah Pauli, Gideon Gießelmann, Michael

Kohlstedt, Judith Becker: investigation, formal analysis; Christina Rohles, Sarah Pauli, Judith Becker, Christoph Wittmann: visualization; Christina Rohles, Sarah Pauli, Judith Becker, Christoph Wittmann: drafting and revising the manuscript; Christoph Wittmann: design of study, conceptualization, supervision, editing, resources, funding acquisition.

Acknowledgements

This work was financially supported by the German Ministry for Education and Research (BMBF) through the grants “BioNylon” (FKZ 03V0757) and “MISSION” (FKZ 031B0611A).

Appendix A. Supplementary data

Supplementary data related to this article can be found at <https://doi.org/10.1016/j.jymben.2022.07.005>.

References

- Adkins, J., Jordan, J., Nielsen, D.R., 2013. Engineering *Escherichia coli* for renewable production of the 5-carbon polyamide building-blocks 5-aminovalerate and glutarate. *Biotechnol. Bioeng.* 110, 1726–1734.
- Barton, N., Horbal, L., Starck, S., Kohlstedt, M., Luzhetskyy, A., Wittmann, C., 2018. Enabling the valorization of guaiacol-based lignin: integrated chemical and biochemical production of *cis,cis*-muconic acid using metabolically engineered *Amycolatopsis* sp ATCC 39116. *Metab. Eng.* 45, 200–210.
- Becker, J., Klopprogge, C., Schröder, H., Wittmann, C., 2009. Metabolic engineering of the tricarboxylic acid cycle for improved lysine production by *Corynebacterium glutamicum*. *Appl. Environ. Microbiol.* 75, 7866–7869.
- Becker, J., Klopprogge, C., Zelder, O., Heinzle, E., Wittmann, C., 2005. Amplified expression of fructose 1,6-bisphosphatase in *Corynebacterium glutamicum* increases *in vivo* flux through the pentose phosphate pathway and lysine production on different carbon sources. *Appl. Environ. Microbiol.* 71, 8587–8596.
- Becker, J., Kuhl, M., Kohlstedt, M., Starck, S., Wittmann, C., 2018a. Metabolic engineering of *Corynebacterium glutamicum* for the production of *cis,cis*-muconic acid from lignin. *Microb. Cell Factories* 17, 115.
- Becker, J., Reinefeld, J., Stellmacher, R., Schäfer, R., Lange, A., Meyer, H., Lalk, M., Zelder, O., von Abendroth, G., Schröder, H., Haefner, S., Wittmann, C., 2013a. Systems-wide analysis and engineering of metabolic pathway fluxes in bio-succinate producing *Basfia succiniciproducens*. *Biotechnol. Bioeng.* 110, 3013–3023.
- Becker, J., Rohles, C.M., Wittmann, C., 2018b. Metabolically engineered *Corynebacterium glutamicum* for bio-based production of chemicals, fuels, materials, and healthcare products. *Metab. Eng.* 50, 122–141.
- Becker, J., Schäfer, R., Kohlstedt, M., Harder, B.J., Borchert, N.S., Stöveken, N., Bremer, E., Wittmann, C., 2013b. Systems metabolic engineering of *Corynebacterium glutamicum* for production of the chemical chaperone ectoine. *Microb. Cell Factories* 12, 110.
- Becker, J., Wittmann, C., 2012. Bio-based production of chemicals, materials and fuels - *Corynebacterium glutamicum* as versatile cell factory. *Curr. Opin. Biotechnol.* 23, 631–640.
- Becker, J., Zelder, O., Hafner, S., Schroder, H., Wittmann, C., 2011. From zero to hero - Design-based systems metabolic engineering of *Corynebacterium glutamicum* for L-lysine production. *Metab. Eng.* 13, 159–168.
- Buschke, N., Becker, J., Schäfer, R., Kiefer, P., Biedendieck, R., Wittmann, C., 2013. Systems metabolic engineering of xylose-utilizing *Corynebacterium glutamicum* for production of 1,5-diaminopentane. *Biotechnol. J.* 8, 557–570.
- Buschke, N., Schröder, H., Wittmann, C., 2011. Metabolic engineering of *Corynebacterium glutamicum* for production of 1,5-diaminopentane from hemicellulose. *Biotechnol. J.* 6, 306–317.
- Cen, X.C., Liu, Y., Chen, B., Liu, D.H., Chen, Z., 2021. Metabolic engineering of *Escherichia coli* for de novo production of 1,5-pentanediol from glucose. *ACS Synth. Biol.* 10, 192–203.
- Chae, T.U., Kim, W.J., Choi, S., Park, S.J., Lee, S.Y., 2015. Metabolic engineering of *Escherichia coli* for the production of 1,3-diaminopropane, a three carbon diamine. *Sci. Rep.* 5, 13040.
- Cheng, J., Tu, W.Y., Luo, Z., Gou, X.H., Li, Q., Wang, D., Zhou, J.W., 2021. A high-efficiency artificial synthetic pathway for 5-aminovalerate production from biobased L-lysine in *Escherichia coli*. *Front. Bioeng. Biotechnol.* 9, 633028.
- Dagorn, A., Chapalain, A., Mijouin, L., Hillion, M., Duclair-Poc, C., Chevalier, S., Taupin, L., Orange, N., Feuilloley, M.G.J., 2013. Effect of GABA, a bacterial metabolite, on *Pseudomonas fluorescens* surface properties and cytotoxicity. *Int. J. Mol. Sci.* 14, 12186–12204.
- Dairo, T.O., Nelson, N.C., Slowing, I.I., Angelici, R.J., Woo, L.K., 2016. Aerobic oxidation of cyclic amines to lactams catalyzed by ceria-supported nanogold. *Catal. Lett.* 146, 2278–2291.
- dos Santos, V.A.P.M., Heim, S., Moore, E.R.B., Stratz, M., Timmis, K.N., 2004. Insights into the genomic basis of niche specificity of *Pseudomonas putida* KT2440. *Environ. Microbiol.* 6, 1264–1286.
- Eggeling, L., Bott, M., 2015. A giant market and a powerful metabolism: L-lysine provided by *Corynebacterium glutamicum*. *Appl. Microbiol. Biotechnol.* 99, 3387–3394.
- Fondi, M., Brilli, M., Emiliani, G., Paffetti, D., Fani, R., 2007. The primordial metabolism: an ancestral interconnection between leucine, arginine, and lysine biosynthesis. *BMC Evol. Biol.* 7, S3.
- Fuhrmann, M., Hausherr, A., Ferbitz, L., Schodl, T., Heitzer, M., Hegemann, P., 2004. Monitoring dynamic expression of nuclear genes in *Chlamydomonas reinhardtii* by using a synthetic luciferase reporter gene. *Plant Mol. Biol.* 55, 869–881.
- Giesselmann, G., Dietrich, D., Jungmann, L., Kohlstedt, M., Jeon, E.J., Yim, S.S., Sommer, F., Zimmer, D., Muhlhaus, T., Schroda, M., Jeong, K.J., Becker, J., Wittmann, C., 2019. Metabolic engineering of *Corynebacterium glutamicum* for high-level ectoine production: design, combinatorial assembly, and implementation of a transcriptionally balanced heterologous ectoine pathway. *Biotechnol. J.* 14, e1800417.
- Gläser, L., Kuhl, M., Jovanovic, S., Fritz, M., Vogeli, B., Erb, T.J., Becker, J., Wittmann, C., 2020. A common approach for absolute quantification of short chain CoA thioesters in prokaryotic and eukaryotic microbes. *Microb. Cell Factories* 19, 160.
- Graf, M., Zieringer, J., Haas, T., Niess, A., Blombach, B., Takors, R., 2018. Physiological response of *Corynebacterium glutamicum* to increasingly nutrient-rich growth conditions. *Front. Microbiol.* 9, 2058.
- Hartmann, M., Tauch, A., Eggeling, L., Bathe, B., Mockel, B., Pühler, A., Kalinowski, J., 2003. Identification and characterization of the last two unknown genes, *dapC* and *dapF*, in the succinylase branch of the L-lysine biosynthesis of *Corynebacterium glutamicum*. *J. Biotechnol.* 104, 199–211.
- Haupt, C., Delepine, B., Irla, M., Heux, S., Wendisch, V.F., 2020. Flux enforcement for fermentative production of 5-aminovalerate and glutarate by *Corynebacterium glutamicum*. *Catalysts* 10, 1065.
- Hoffmann, S.L., Jungmann, L., Schiefelbein, S., Peyriga, L., Cahoreau, E., Portais, J.C., Becker, J., Wittmann, C., 2018. Lysine production from the sugar alcohol mannitol: design of the cell factory *Corynebacterium glutamicum* SEA-3 through integrated analysis and engineering of metabolic pathway fluxes. *Metab. Eng.* 47, 475–487.
- Hoffmann, S.L., Kohlstedt, M., Jungmann, L., Hutter, M., Poblete-Castro, I., Becker, J., Wittmann, C., 2021. Cascaded valorization of brown seaweed to produce L-lysine and value-added products using *Corynebacterium glutamicum* streamlined by systems metabolic engineering. *Metab. Eng.* 67, 293–307.
- Hong, J., Kim, K.J., 2019. Crystal structure of gamma-aminobutyrate aminotransferase in complex with a PLP-GABA adduct from *Corynebacterium glutamicum*. *Biochem. Biophys. Res. Commun.* 514, 601–606.
- Joo, J.C., Oh, Y.H., Yu, J.H., Hyun, S.M., Khang, T.U., Kang, K.H., Song, B.K., Park, K., Oh, M.K., Lee, S.Y., Park, S.J., 2017. Production of 5-aminovaleric acid in recombinant *Corynebacterium glutamicum* strains from a *Miscanthus* hydrolysate solution prepared by a newly developed *Miscanthus* hydrolysis process. *Bioresour. Technol.* 245, 1692–1700.
- Jorge, J.M.P., Perez-García, F., Wendisch, V.F., 2017. A new metabolic route for the fermentative production of 5-aminovalerate from glucose and alternative carbon sources. *Bioresour. Technol.* 245, 1701–1709.
- Kind, S., Jeong, W.K., Schröder, H., Wittmann, C., 2010. Systems-wide metabolic pathway engineering in *Corynebacterium glutamicum* for bio-based production of diaminopentane. *Metab. Eng.* 12, 341–351.
- Kind, S., Kreye, S., Wittmann, C., 2011a. Metabolic engineering of cellular transport for overproduction of the platform chemical 1,5-diaminopentane in *Corynebacterium glutamicum*. *Metab. Eng.* 13, 617–627.
- Kind, S., Kreye, S., Wittmann, C., 2011b. Metabolic engineering of cellular transport for overproduction of the platform chemical 1,5-diaminopentane in *Corynebacterium glutamicum*. *Metab. Eng.* 13, 617–627.
- Kind, S., Neubauer, S., Becker, J., Yamamoto, M., Völkert, M., Abendroth, G.V., Zelder, O., Wittmann, C., 2014. From zero to hero - production of bio-based nylon from renewable resources using engineered *Corynebacterium glutamicum*. *Metab. Eng.* 25, 113–123.
- Kohlstedt, M., Weimer, A., Weiland, F., Stolzenberger, J., Selzer, M., Sanz, M., Kramps, L., Wittmann, C., 2022. Biobased PET from lignin using an engineered *cis,cis*-muconate-producing *Pseudomonas putida* strain with superior robustness, energy and redox properties. *Metab. Eng.* 72, 337–352.
- Krömer, J.O., Sorgenfrei, O., Klopprogge, K., Heinzle, E., Wittmann, C., 2004. In-depth profiling of lysine-producing *Corynebacterium glutamicum* by combined analysis of the transcriptome, metabolome, and fluxome. *J. Bacteriol.* 186, 1769–1784.
- Lange, A., Becker, J., Schulze, D., Cahoreau, E., Portais, J.C., Haefner, S., Schröder, H., Krawczyk, J., Zelder, O., Wittmann, C., 2017. Bio-based succinate from sucrose: high-resolution ¹³C metabolic flux analysis and metabolic engineering of the rumen bacterium *Basfia succiniciproducens*. *Metab. Eng.* 44, 198–212.
- Li, Z., Xu, J., Jiang, T.T., Ge, Y.S., Liu, P., Zhang, M.M., Su, Z.G., Gao, C., Ma, C.Q., Xu, P., 2016. Overexpression of transport proteins improves the production of 5-aminovalerate from L-lysine in *Escherichia coli*. *Sci. Rep.* 6, 30884.
- Liu, P., Zhang, H., Lv, M., Hu, M., Li, Z., Gao, C., Xu, P., Ma, C., 2014. Enzymatic production of 5-aminovalerate from L-lysine using L-lysine monooxygenase and 5-aminovaleramide amidohydrolase. *Sci. Rep.* 4, 5657.
- Marienhagen, J., Kennerknecht, N., Sahn, H., Eggeling, L., 2005. Functional analysis of all aminotransferase proteins inferred from the genome sequence of *Corynebacterium glutamicum*. *J. Bacteriol.* 187, 7639–7646.
- McCraw, S.L., Park, D.H., Jones, R., Bentley, M.A., Rico, A., Ratcliffe, R.G., Kruger, N.J., Collmer, A., Preston, G.M., 2016. GABA (gamma-aminobutyric acid) uptake via the GABA permease *GabP* represses virulence gene expression in *Pseudomonas syringae* pv. tomato DC3000. *Mol. Plant Microbe Interact.* 29, 938–949.

- Miller, D.L., Rodwell, V.W., 1971. Metabolism of basic amino acids in *Pseudomonas-putida* - catabolism of lysine by cyclic and acyclic Intermediates. *J. Biol. Chem.* 246, 2758.
- Noe, F.F., Nickerson, W.J., 1958. Metabolism of 2-pyrrolidone and gamma-aminobutyric acid by *Pseudomonas aeruginosa*. *J. Bacteriol.* 75, 674–681.
- Park, S.J., Kim, E.Y., Noh, W., Park, H.M., Oh, Y.H., Lee, S.H., Song, B.K., Jegal, J., Lee, S. Y., 2013. Metabolic engineering of *Escherichia coli* for the production of 5-aminovaleate and glutarate as C₅ platform chemicals. *Metab. Eng.* 16, 42–47.
- Park, S.J., Oh, Y.H., Noh, W., Kim, H.Y., Shin, J.H., Lee, E.G., Lee, S., David, Y., Baylon, M.G., Song, B.K., Jegal, J., Lee, S.Y., Lee, S.H., 2014. High-level conversion of L-lysine into 5-aminovaleate that can be used for nylon 6,5 synthesis. *Biotechnol. J.* 9, 1322–1328.
- Pavic, A., Ji, Y., Serafini, A., Garza-Garcia, A., McPhillie, M.J., Holmes, A.O.M., de Carvalho, L.P.S., Wang, Y., Bartlam, M., Goldman, A., Postis, V.L.G., 2021. Functional characterization of the gamma-aminobutyric acid transporter from *Mycobacterium smegmatis* MC(2) 155 reveals sodium-driven GABA transport. *J. Bacteriol.* 203, e00642–20.
- Perez-Garcia, F., Wendisch, V.F., 2018. Transport and metabolic engineering of the cell factory *Corynebacterium glutamicum*. *FEMS Microbiol. Lett.* 365, fny166.
- Richard, H.T., Foster, J.W., 2003. Acid resistance in *Escherichia coli*. *Adv. Appl. Microbiol.* 52, 167–186, 52.
- Rohles, C.M., Giesselmann, G., Kohlstedt, M., Wittmann, C., Becker, J., 2016. Systems metabolic engineering of *Corynebacterium glutamicum* for the production of the carbon-5 platform chemicals 5-aminovaleate and glutarate. *Microb. Cell Factories* 15, 154.
- Rohles, C.M., Glaser, L., Kohlstedt, M., Giesselmann, G., Pearson, S., del Campo, A., Becker, J., Wittmann, C., 2018. A bio-based route to the carbon-5 chemical glutaric acid and to bionylon-6,5 using metabolically engineered *Corynebacterium glutamicum*. *Green Chem.* 20, 4662–4674.
- Schneider, F., Kramer, R., Burkovski, A., 2004. Identification and characterization of the main beta-alanine uptake system in *Escherichia coli*. *Appl. Microbiol. Biotechnol.* 65, 576–582.
- Shang, X.L., Zhang, Y., Zhang, G.Q., Chai, X., Deng, A.H., Liang, Y., Wen, T.Y., 2013. Characterization and molecular mechanism of AroP as an aromatic amino acid and histidine transporter in *Corynebacterium glutamicum*. *J. Bacteriol.* 195, 5334–5342.
- Shi, F., Si, H., Ni, Y.L., Zhang, L., Li, Y.F., 2017. Transaminase encoded by NCg12515 gene of *Corynebacterium glutamicum* ATCC13032 is involved in gamma-aminobutyric acid decomposition. *Process Biochem.* 55, 55–60.
- Shin, J.H., Park, S.H., Oh, Y.H., Choi, J.W., Lee, M.H., Cho, J.S., Jeong, K.J., Joo, J.C., Yu, J., Park, S.J., Lee, S.Y., 2016. Metabolic engineering of *Corynebacterium glutamicum* for enhanced production of 5-aminovaleic acid. *Microb. Cell Factories* 15, 174.
- Shin, J.H., Park, S.J., Lee, S.Y., 2014. Metabolic engineering of *Corynebacterium glutamicum* for production of 5-aminovaleic acid and glutaric acid as C₅ platform chemicals. *New Biotechnol.* 31, S162.
- Sohn, Y.J., Kang, M., Baritugo, K.A., Son, J., Kang, K.H., Ryu, M.H., Lee, S., Sohn, M., Jung, Y.J., Park, K., Park, S.J., Joo, J.C., Kim, H.T., 2021. Fermentative high-level production of 5-hydroxyvaleric acid by metabolically engineered *Corynebacterium glutamicum*. *ACS Sustain. Chem. Eng.* 9, 2523–2533.
- Tunncliff, G., 1993. Inhibition of 4-aminobutyrate aminotransferase from *Pseudomonas fluorescens* by ATP. *Biochem. Mol. Biol. Int.* 31, 41–47.
- van Duuren, J., de Wild, P.J., Starck, S., Bradtmoller, C., Selzer, M., Mehlmann, K., Schneider, R., Kohlstedt, M., Poblete-Castro, I., Stolzenberger, J., Barton, N., Fritz, M., Scholl, S., Venus, J., Wittmann, C., 2020. Limited life cycle and cost assessment for the bioconversion of lignin-derived aromatics into adipic acid. *Biotechnol. Bioeng.* 117, 1381–1393.
- Vandecasteele, J.P., Hermann, M., 1972. Regulation of a catabolic pathway - lysine degradation in *Pseudomonas putida*. *Eur. J. Biochem.* 31, 80–85.
- Vardon, D.R., Franden, M.A., Johnson, C.W., Karp, E.M., Guarnieri, M.T., Linger, J.G., Salm, M.J., Strathmann, T.J., Beckham, G.T., 2015. Adipic acid production from lignin. *Energy Environ. Sci.* 8, 617–628.
- von Tiedemann, P., Anwar, S., Kemmer-Jonas, U., Asadi, K., Frey, H., 2020. Synthesis and solution processing of nylon-5 ferroelectric thin films: the renaissance of odd-nylons? *Macromol. Chem. Phys.* 221, 1900468.
- Wan, Y., Kertesz, M., Spitale, R.C., Segal, E., Chang, H.Y., 2011. Understanding the transcriptome through RNA structure. *Nat. Rev. Genet.* 12, 641–655.
- Wang, X., Cai, P.P., Chen, K.Q., Ouyang, P.K., 2016. Efficient production of 5-aminovaleate from L-lysine by engineered *Escherichia coli* whole-cell biocatalysts. *J. Mol. Catal. B Enzym.* 134, 115–121.
- Wittmann, C., Heinze, E., 2001. Modeling and experimental design for metabolic flux analysis of lysine-producing corynebacteria by mass spectrometry. *Metab. Eng.* 3, 173–191.
- Wittmann, C., Krömer, J.O., Kiefer, P., Binz, T., Heinze, E., 2004. Impact of the cold shock phenomenon on quantification of intracellular metabolites in bacteria. *Anal. Biochem.* 327, 135–139.
- Xu, Y.Q., Zhou, D., Luo, R.S., Yang, X.Z., Wang, B.S., Xiong, X.C., Shen, W.F., Wang, D., Wang, Q.H., 2020. Metabolic engineering of *Escherichia coli* for polyamides monomer delta-valerolactam production from feedstock lysine. *Appl. Microbiol. Biotechnol.* 104, 9965–9977.
- Zhao, Z., Ding, J.Y., Li, T., Zhou, N.Y., Liu, S.J., 2011. The ncgl1108 (PheP(Cg)) gene encodes a new L-Phe transporter in *Corynebacterium glutamicum*. *Appl. Microbiol. Biotechnol.* 90, 2005–2013.
- Zhao, Z., Ding, J.Y., Ma, W.H., Zhou, N.Y., Liu, S.J., 2012. Identification and characterization of gamma-aminobutyric acid uptake system GabPCg (NCgl0464) in *Corynebacterium glutamicum*. *Appl. Environ. Microbiol.* 78, 2596–2601.